NANO EXPRESS

OPEN ACCESS

RECEIVED
28 June 2020

REVISED
12 August 2020

ACCEPTED FOR PUBLICATION
1 September 2020

PUBLISHED
15 September 2020

TOPICAL REVIEW

Advances in mechanical characterization of 1D and 2D nanomaterials: progress and prospects

Maria F Pantano[1,3] **and Irma Kuljanishvili**[2,3]

[1] Department of Civil, Environmental and Mechanical Engineering, University of Trento, Via Mesiano 77, 38123 Trento, Italy
[2] Department of Physics, Saint Louis University, St. Louis, Missouri, 63103, United States of America
[3] Authors to whom any correspondence should be addressed.

E-mail: maria.pantano@unitn.it **and** irma.kuljanishvili@slu.edu

Keywords: 1D and 2D nanomaterials, mechanical properties, MEMS, nanomanipulation, nanofabrication

Abstract

Last several decades have sparked a tremendous interest in mechanical properties of low dimensional systems specifically 1D and 2D nanomaterials, in large, due to their remarkable behavior and potential to possess unique and customizable physical properties, which have encouraged the fabrication of new structures to be tuned and utilized for targeted applications. In this critical review we discuss examples that represent evolution of the mechanical characterization techniques developed for 1D and 2D nanomaterials, with special emphasis on specimen fabrication and manipulation, and the different strategies, tools and metrologies, employed for precise positioning and accurate measurements of materials' strength, elastic modulus, fracture toughness as well as analysis of failure modes. We focus separately on techniques for the mechanical characterization of 1D and 2D nanomaterials and categorize those methods into top-down and bottom-up approaches. Finally, we discuss advantages and some drawbacks in most common methodologies used for 1D and 2D specimen testing and outline future possibilities and potential paths that could boost the development of more universal approaches for technologically viable solutions which would allow for more streamlined and standardized mechanical testing protocols to be developed and implemented.

1. Introduction

The interest towards low dimensional nanoscale materials received a big boost in the early 1990s with the discovery of single walled carbon nanotubes (SWCNTs), which, soon after, sparked the excitement in the scientific community for other types of 1D nanostructures, such as semiconducting or metallic nanorods and nanowires. Later, in the early 2000s, the family of nanomaterials further grew, and soon after, the isolation of the first single layer carbon (e.g., graphene) unveiled the possibility to synthetize an entire class of layered van der Waals nanomaterials that now have become front and center of a new era in technological advancements.

Low dimensional nanoscale materials such as nanowires, nanotubes, (1D nanostructures) as well as atomically thin and ultra-thin films (2D layered materials) display fascinating optical, electrical, thermal and mechanical properties that go well beyond those of classical bulk materials [1–5]. One of the most intriguing aspects of these materials is related to the unmatched mechanical properties, where, for example, graphene excels with a record strength (130 GPa) and Young's modulus (1 TPa), and outperforms any previously reported material including carbon nanotubes [6].

Novel functions and performances [7], including multifunctionality or prolonged lifetime in extreme environments, could emerge from the implementation of 1D and 2D nanomaterials into composite structures [8, 9], electronic devices [10, 11], flexible electronics [12–14], batteries [15] and biosensors [16], just to mention few possible applications. Furthermore, novel materials can be fabricated from the bottom-up with tailored properties [17]. Typical examples are, for instance, multilayer stacks, where single atomic layers are one on top of the other and held together by Van der Waals interactions [18, 19]. In current designs, either 1D and 2D materials can be found as reinforcement components or mixed together in more complex composite systems.

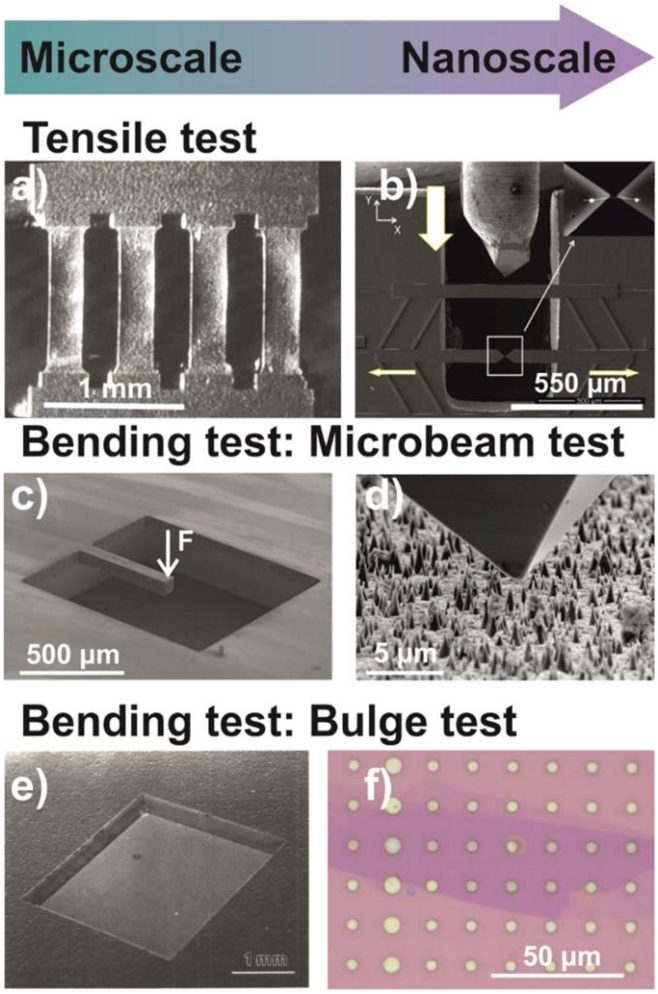

Figure 1. Comparison between specific mechanical testing configurations (tensile test, microbeam and bulge test) implemented for microscale and nanoscale material samples. (a) Reprinted with permission from [31]. Copyright 1993, Materials Research Society; (b) Reprinted with permission from [32]. Copyright 2009, Society for Experimental Mechanics; c) Reprinted with permission from [33]. Copyright 2008, Elsevier Ltd; (d) Reprinted with permission from [34]. Copyright 2006, American Chemical Society; (e) Reprinted with permission from [35]. Copyright 1992, Materials Research Society; (f) Reprinted with permission from [36]. Copyright 2011, Springer Nature.

With regards to this latter class of materials, it was shown that the combination of nanosheets with nanowires or nanotubes results in improved electrochemical properties for battery applications [20–22] or toughness enhancement of 2D layers [23, 24].

In order to exploit the great potential of nanostructures into manipulable, high-performance devices, it is necessary to achieve better and more comprehensive understanding of their mechanical properties, such as strength, Young's modulus and fracture strain, toughness while taking into account differences in their methods of preparation, fabrication and testing apparatuses. Because mechanical loading always accompanies devices in their normal operation, the capability of a given structure to withstand bending, stretching or twisting is a key factor for achieving satisfactory performance, required reliability and prolonged lifetime. Given their specific topology, traditional mechanical testing systems are not very appropriate for testing structures whose characteristic length develops at the nanoscale, therefore specific methodologies have been implemented so far to accommodate small length scales; as well summarized in these review articles [25–29].

Historically speaking, in the past half a century [30], mechanical testing of microscale structures, such as whiskers, microbeams or micromembranes, has been done via employments of custom built stages and devices. Those allowed for tensile tests, bending, compression, buckling, torsional or resonance tests, in order to determine valuable mechanical properties. Some of those readily available solutions were considered from previous generation microscale-platforms, and subsequently developed in testing apparatuses for mechanical characterization of 1D and 2D nanomaterials (figure 1).

Novel and nanoscale-specific strategies for sample preparation, deposition/mounting and gripping have been developed along with new testing apparatuses. In the following sections, we will briefly describe most commonly used methods for sample preparation as well as list testing tools used to mechanically characterize 1D

and 2D nanomaterials. Here we review the main testing platforms which were used and how they evolved in recent decades. Finally, we will categorize two general approaches in the mechanical characterization, namely top-down versus bottom-up approach, describing major advantages and outlining existing challenges in both methodologies.

2. One-dimensional nanomaterials (nanowires, nanorods and nanotubes) and their mechanical characterization

A wide variety of high aspect ratio one-dimensional nanostructures have been investigated in the past several decades, which include micrometers long and 1–2 nm in diameter single walled carbon nanotubes (SWCNTs) to multiwall carbon nanotubes (MWCTs) with diameter from 50 nm up to 100 nm, as well as various semiconductor nanowires (such as zinc oxide (ZnO), Si, silicon carbide (SiC), gallium nitride (GaN), boron nitride (BN) and tin oxide (SnO_2) nanowires [37–44]), metallic nanorods (such as Nb, Ag or Pd nanowires [45–49]), or diamond nano-niddles [4].

In mechanical characterization of 1D nanowires or nanotubes the main task is to isolate an individual specimen and mount it onto the testing stage or tool. Handling 50 nm–100 nm diameter wires versus 1–2 nm nanotubes often presents different technical issues. Depending on the methods of synthesis, usually, nanowires or nanotubes are in the form of yarns, powders, dispersed in suspensions, or assembled naturally on the growth substrate, etc. So customarily different tools are employed first, (a) for isolating and mounting a specimen on the testing stage and next, (b) for testing. Regarding the experimental setups, two predominant approaches include: (a) piezo-driven high-precision systems, such as atomic force microscopy (AFM) and nanoindentation, and (b) complete miniaturized actuation/sensing platforms based on microelectromechanical systems (MEMS) technology. Although both approaches have been used successfully in testing 1D systems, latter has been gaining attention in the recent years because of a more streamlined sample preparation.

2.1. Growth methods and synthesis techniques of 1D nanomaterials

High aspect ratio one-dimensional nanostructures are most often prepared either in a forest- like vertical orientation, monolayer to few layer networks or multi-layered dense mats, isolated individually or in very low density arrangements through selective catalytic growth, or via etching or milling. Methods of synthesis range from relatively low temperature hydrothermal techniques to various intermediate temperature chemical or physical vapor deposition (CVD or PVD), or relatively high temperature laser ablation techniques just to name a few [50–55].

2.1.1. Carbon-based 1D nanomaterials (carbon nanotubes)

One of the most exciting examples of 1D nanomaterials are carbon nanotubes, in their variety of diameters as well as morphologies, which include nano-ropes, nano-yarns and nano-needles, etc. Regarding the synthesis process, in particular, high temperature low-pressure arc-discharge method has been known to produce highest quality single walled or multiwall carbon nanotubes. Catalytic chemical vapor deposition has on the other hand provided a great alternative for CNTs production with controlled geometries yet allowing good quality material synthesis in ambient pressures. More importantly, with catalytic CVD methods CNTs can be produced not only in a controlled predefined manner, but also in a scalable fashion and in ambient environments, relatively inexpensively, as compared to other high vacuum methods.

In the study of mechanical properties of carbon nanotubes, Ganesan *et al* [48], compared two types of CNTs, specifically MWCNTs, pristine and nitrogen doped, prepared by catalytic chemical vapor deposition CVD. In this study authors describe that pristine mw-CNT specimens were grown on quartz substrates by injecting a mixture of 20 mg ml^{-1} of ferrocene ($(C_5H_5)_2Fe$) in xylene (C_8H_{10}) solution into a two-stage thermal CVD reactor consisting of a low temperature (200 °C) pre-heater region followed by a higher temperature main reactor (775 °C). Similarly carbon nanotubes were also prepared using a mixture of xylene and acetonitrile (CH_3CN) as the carbon/nitrogen source. Authors found that pristine and N-doped carbon nanotubes exhibited different load-bearing abilities, because of their different wall structures. A small amount of solution from a sonicated suspension of the MWCNTs in toluene was deposited onto a Si wafer coated with a 5 nm thick layer of titanium. Individual MWNTs, that were about 10 μm in length and 70–100 nm in diameter, were subsequently picked up and placed across the shuttles of the testing device, coated with epoxy, using micromanipulators. The epoxy layer, upon hardening, acted as a clamp for the tensile specimens, measurements were performed within *in situ* SEM equipped with indenter used as load applicator.

Single walled nanotubes have also been investigated. Most studies of mechanical properties of SWCNTs [56, 57] were done on CNTs ropes or bundles, and only few works have been reported on individual SWCNTs [58, 59]. In the studies of Salvetat *et al* [56], and Yu *et al* [57], SWCNTs ropes were investigated. In both studies

specimens were produced by arc-discharge methods following standard well-established purification process involving acid treatments and filtration. *Selvetat et al* prepared ropes in liquid suspension and mixing the soot in ethanol and dispensing the droplet of the suspension over a polished alumina membrane with 200 nm pores. Occasional SWCNT ropes were found suspended over the membrane pore, which were then considered for mechanical testing. In the study by Yu *et al* [57], SWCNTs were also prepared by the laser ablation method and purified by refluxing and filtration. Single ropes projecting from a so called 'SWCNTs- paper' were then attached at their free end to an AFM tip through deposition of carbonaceous material. Regarding the tensile testing of individual SWCNTs, the first report dates back to 2010 by Wang *et al* [58]. In this case, stock MWCNTs initially produced by arc-discharge method were mounted between a W-tip and conductive AFM cantilever, and through a consecutive electrical breaking down of the outer shells of the MWCNTs until single shell segment of inner CNTs was exposed and observed via high resolution Transmission Electron Microscope (HRTEM). Very recently, Takakura *et al* [59] studied the relationship between the tensile strength of SWCNTs and their structural (chiral) differences. Individual SWCNTs of different chilarities were identified using broadband Rayleigh scattering and used in the measurements. Specimens were grown by CVD on the open-slit substrates with average lengths in tens of micrometers and diameters ranging from 1.3–3 nm. Selected SWCNTs were then picked up by micro-fork and placed onto a custom-made MEMS tensile testing device. Manipulation of the SWCNTs was done *in situ* Scanning Electron Microscope (SEM) and electron-beam induced deposition (EBID) was used to deposit Pt clamps to hold down the specimen.

Details about the mechanical properties of the materials mentioned above are reported in section 2.2.

2.1.2. Semiconducting 1D nanomaterials

Regarding the fabrication of semiconducting 1D nanomaterials, for example ZnO nanowires (NWs), several methods of synthesis are available, those include: physical (sputtering, thermal, or atomic layer deposition) and chemical methods of growth, such as solution based syntheses or vapor-liquid-solid (VLS), or vapor-solid (VS) methods [52, 60–64]. It is useful to note that process of growth whether it is VLS or VS is governed largely by the nature of catalyst particle or surface, its physical condition, size or other surface physical properties.

The most common techniques for ZnO production, can be categorized as vapor based or solutions based methods. Examples of which are hydrothermal-solution-based growth methods and CVD synthesis methods on various substrates, including substrates such as single crystal sapphire or other single crystal substrates that promote the growth of aligned nanowires forests [39].

In solution based methods, such as hydrothermal methods, synthesis takes place usually in a solution-bath, and the growth process (at relatively low T $\sim$ 150–170 °C) often requires 24 up to 48 hours to complete, including both precursor preparation and synthesis itself. Chemical vapor deposition process on the other hand is performed usually at much higher temperature ~780–850 °C at ambient pressure. Common catalyst used in CVD production of ZnO NWs are Au, other catalysts such as Fe, Ni and Co have also been tested and reported [65, 66].

Apart from custom-grown samples, tests on commercially purchased ZnO nanowires were also reported. For example, Agrawal *et al* [40] studied commercially purchased ZnO NWs, which were dispersed in alcohol suspension and drop casted onto the TEM grid; then single NW was moved onto MEMS device using micro-manipulators inside of a SEM, where Pt electrodes were sputtered *in situ* prior to testing.

In two separate studies Chang *et al* [39], and Zhang *et al* [38] prepared and studied SiC NWs and Si NWs respectively. NWs were grown using vapor-liquid solid method. SiC NWs [43] and doped Si NWs [42], with the diameters ranging from 20 to 200 nm with the typical length of ~18 μm, respectively were grown using vapor-liquid solid method, and tests were performed on MEMS devices. Silicon carbide NWs were grown at 800 °C with Fe as catalyst and C and SiO_2 as source precursors and all materials were used in powdered form. Doped Si-NWs were prepared/grown using mix of SiH_4 source gas, and single crystal Si $\langle 111 \rangle$ wafer used at 500 °C growth temperature and for 40 min, at 0.5 mbar pressure. Prior to the growth, wafer was annealed at 650 °C for 10 min in high vacuum ($\sim 1 \times 10^{-7}$ mbar). *In situ* doping was achieved during the growth by adding 2% phosphine (PH_3) into the process gas mix. It is important to note that the mounting and/or transfer of individual Si-NWs or SiC NTs directly onto MEMS device was done using SEM and *in situ* micromanipulators and nanowires were generally clamped to their respective measuring stage using some form of nanowelding through focused ion beam (FIB).

In another study [41], Brown *et al* measured the tensile strength of Si doped GaN single crystal NWs which were prepared using plasma assisted molecular beam epitaxy method (PAMBE). The nanowire-liquid-suspension was prepared by brief sonication of host support-substrate for few minutes, and then NW containing liquid suspension was dispersed using syringe that was positioned over the MEMS testing device using a probe station micro-manipulator. Then randomly oriented GaN NWs were integrated with active (MEMS) devices using dielectrophoresis-driven self-assembly, and platinum-carbon clamps were created using a gallium focused ion beam via *in situ* SEM. This dielectrophoresis method is considered less time consuming as compared to

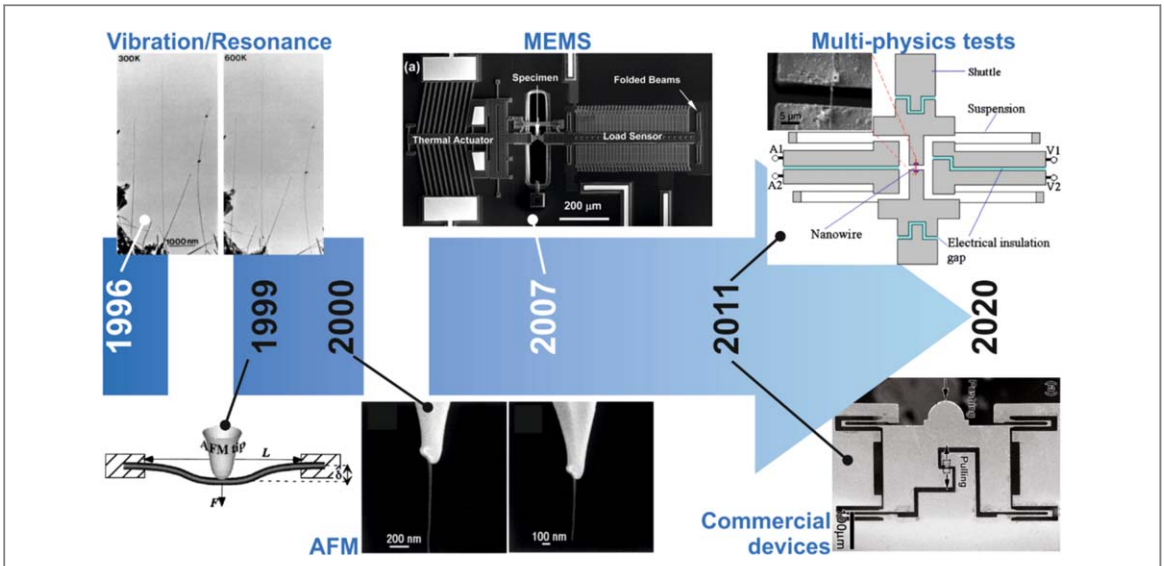

Figure 2. Milestones in the mechanical characterization of 1D nanomaterials. In the late 1990s, the mechanical properties of multi-walled carbon nanotubes and single-walled carbon nanotubes ropes were investigated by resonance/vibration methods (Reprinted with permission from [71]. Copyright 1996, Springer Nature), AFM bending tests (Reprinted with permission from [56]. Copyright 1999, American Physical Society). In 2000, a tensile test was conducted on single-walled carbon nanotube ropes by the means of an AFM (Reprinted with permission from [57]. Copyright 2000, American Physical Society). In the second half of the 2000s, different research groups started developing custom-made MEMS testing platforms that allowed *in situ* SEM/TEM tensile testing of nanotubes and nanowires (Reprinted with permission from [40]. Copyright 2008, American Chemical Society). At the beginning of the 2010s, there were the first applications of commercial devices for *in situ* testing of nanostructures [72]. Copyright 2011, American Chemical Society. Contemporarily, the MEMS-based tensile testing platforms evolved and incorporated additional functionalities in order to perform multi-physics tests. For example, piezoresistivity properties of silicon nanowires were tested [73] (Reprinted with permission from [74] Copyright 2009, IOP Publishing).

other methods where individual NWs are placed on MEMS devices using micromanipulators one at a time. In dielectrophresis methods two electrical probes are placed in contact with metal pads that allow an alternating (AC) electrical field to be applied across the fixed and moving stages, creating a gradient of the electric field amplitude which subsequently aligns/polarizes nanowires that eventually bridge the gap between the fixed and moving stages. This is a known method for integrating nanowires derived from liquid suspensions into micro-fabricated structures, in general.

In two separate studies Zetl *et al* [37] and Wei *et al* [38], reported on the BN nanotubes. Those one dimensional nanostructures can be described as structurally similar to carbon nanotubes with alternating B and N atoms substituting for C atoms in a hexagonal (honeycomb) lattice.

In the earlier study by Zetl *et al* individual mw-BNNTs were prepared by arc-discharge method using BN filled tungsten. The BNNTs synthesized with arc-discharge method are of high purity, although such BNNTs are often terminated by metal particles. Presence of metal nanoparticles was subsequently taken into account in analyses which resulted in estimated decreased fundamental frequency of thermally oscillating NT by 17%, while leaving elastic modulus unchanged.

2.1.3. Metallic 1D nanomaterials

Metallic 1D nanomaterials are now attracting interest in several fields, such as electrodes for flexible electronics, superconductive circuit element and devices, as well as efficient materials for antennas and receivers in electromagnetic environments [67, 68]. Here we will consider three representative materials, such as Ag, Nb and Pd nanowires, which were recently studied from a mechanical point of view. Experimental tensile studies on single crystal metallic Ag nanowires were reported by Filleter *et al* [47], where Ag NWs (5–10 μm long and with diameters ranging from 40 to 120 nm) were prepared by a modified polyol route as follows: a solution of 55 000 MW polyvinylpyrrolidone (PVP) in ethylene glycol (5 ml, 40 mg ml^{-1}) was refluxed at 170 °C in a hot oil bath, steered and then NaCl in ethylene glycol (150 μl, 2.87 mg ml^{-1}) was added to the solution, followed by $AgNO_3$ in ethylene glycol (50 μl, 25 mg ml^{-1}), temperature of the mix was kept the same, for 15 min after which, color of the solution turned yellow, indicating seed-particle formation. Next $AgNO_3$ in ethylene glycol (1 ml, 25 mg ml^{-1}) was added and reacted for 12 more minutes, after which the mix shows indication of resulting in a gray mixed suspension containing nanowires, as well as other nanorods and nanoparticles. PVP surface capping agent usually covers the surface of the nanowires, and other nanoscale byproducts nanorods and nanoparticles, that did not grow into high- aspect ratio nanowires.

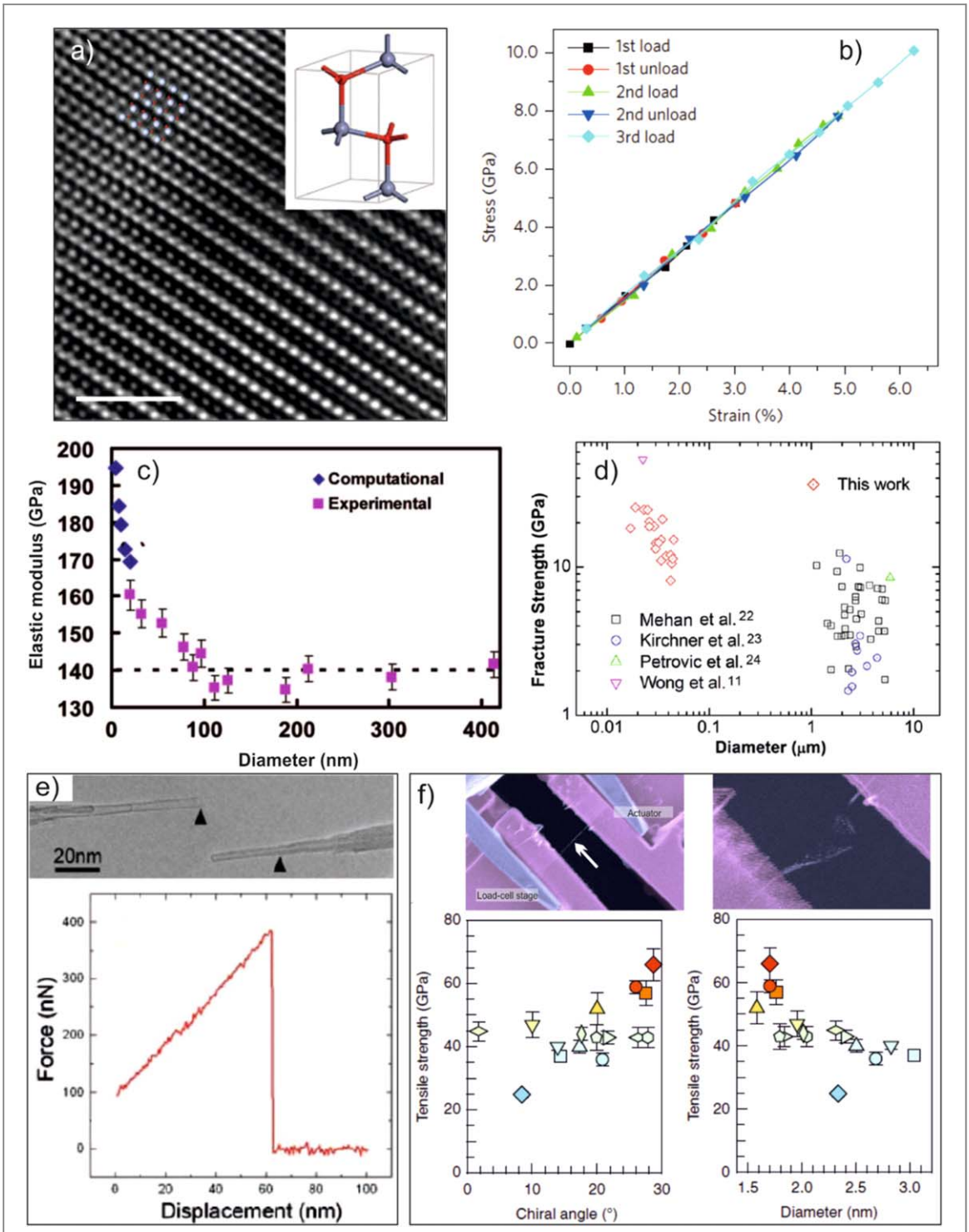

Figure 3. (a) HRTEM image shows a perfect atomic arrangement in the close-packed layers of {0001}. Inset: atomic model of a ZnO unit cell. Scale bar, 2 nm. Reprinted with permission from [45]. Copyright 2015, Springer Nature; (b) Stress-strain curve of a ZnO nanowire. Reprinted with permission from [45]. Copyright 2015, Springer Nature; (c) Dependence of the Young's modulus of GaN nanowires on their diameter. Reprinted with permission from [40]. Copyright 2008, American Chemical Society; (d) Dependence of strength of SiC nanowires with size. Reprinted with permission from [43]. Copyright 2014, American Chemical Society; (e) Force-displacement curve of a single-walled carbon nanotube. Failure occurred far from the SWNT/MWNT joint region. Reprinted with permission from [58]. Copyright 2010, Wiley-VCH Verlag GmbH & Co.; (f) Positioning and failure of a single-walled carbon nanotube onto a MEMS-based tensile testing device. Its tensile strength plotted as a function of both the chiral angle and diameter. Reprinted under the terms of the Creative Commons CC BY license from [59]. Copyright 2019, Springer Nature.

Recently, excellent mechanical properties were reported in Nb nanowires by Wang *et al* [46]. In this study test specimens Nb nanowires (with diameters ranging from 10 to 30 nm) were prepared via *in situ* nanoscale welding inside the TEM. In this process, two nano-tips with specific orientations on the fracture surface of the two Nb rods (0.25 mm), were connected together using a piezo-manipulator, thus forming a single-crystal or bi-crystal by applying 20 ns square electric pulses, of 0.7 to 1.4 Volts amplitudes.

Finally, thermal evaporation can be used for the synthesis of metallic single-crystal 1D structures, such as high purity Pd nanowhiskers at high temperature (~1200 °C), and ultra-high vacuum conditions [69, 70]. Here Pd nanowhiskers were produced on $SrTiO_3$ coated Si substrate and transferred onto MEMS device under SEM conditions via manipulators. The NW axes oriented along ⟨110⟩ crystallographic directions, with lengths around (5 to 20 μm) and diameters of about 30 to 150 nm. Individual nanowires were then loaded under tension at different temperature and strain rate conditions to evaluate dislocation nucleation strengths.

2.2. Overview of the testing platforms for mechanical characterization of 1D materials

Different testing platforms have been developed over the years (figure 2) for the mechanical characterization of a wide variety of 1D nanostructures, such as nanotubes, nanowires, nanorods and nanoniddles (figure 3). While in the late 1990s bending test configurations were the first to appear, later researchers, for the most part, have moved toward the tensile tests.

One of the first reported methods was based on the study of the vibration modes of isolated MWCNTs and BNNTs under thermal loading *in situ* TEM [37, 71] as shown in figure 2, (corresponding to 1996). Such tests allowed to derive the first estimation of the Young's modulus, which on average resulted to be 1.8 TPa [71] for MWCNT and 1.22 $\pm$ 0.24 TPa [37] for BN multi-walled nanotubes, respectively. BNNT Young's modulus (1.22 TPa) was estimated to be 14 times greater than the in-plane modulus of the bulk hBN, which authors attributed to an extremely high crystallinity and purity of BNNT as compared to bulk layers.

Later, a pioneering study in the mechanical characterization of carbon nanotubes reported the performance of a tensile test through a couple of AFM tips. In this case, the sample of interest, such as MWCNT, was manipulated between two AFM probes with different cantilever stiffness. In particular, one behaved more as a rigid probe and applied the displacement to the sample, while the other one was sufficiently soft and able to bend as a tensile load was applied to the specimen. From the deflection of the soft probe, it was then possible to derive both the load and the displacement experienced by the sample [56, 57]. In this way, a stress-strain curve of the nanosample could be derived and from this a full set of mechanical properties. In this case, the Young's modulus, the strength and the strain at failure resulted to be in the range of 1.4–2.9 TPa, 18–68 GPa and about ~2 to 12%, respectively. A similar setup, including a compliant AFM cantilever and a rigid tip, connected in this case to a piezoelectric tube drive, was implemented later to determine the mechanical response (i.e., full stress-strain curve) of individual multi-walled boron nitride nanotubes under tensile loading or pull-out experiments [38] inside HRTEM equipped with an integrated AFM system incorporated within a side-entry TEM holder. In this study the specimen, individual BNNT, was mounted between AFM cantilever (tip) and piezo-driven retractable tungsten tip mounted inside the TEM -AFM holder. This allows to measure AFM cantilever deflection, (Δx) and the length of the BNNT. By measuring the applied forces and tube lengths until breakage, authors obtained real stress-strain curves, from which the Young's modulus (in the range of 0.725–1.343 TPa), as well as the ultimate tensile strengths and strains were calculated. More difficulties were related to the extraction of both the strength (33.2 GPa) and the breaking strain (3.4%), as many specimens broke at the clamp.

Regarding single-walled carbon nanotubes, they were mostly characterized in the shape of ropes [56, 57]. For example, in [56] SWCNTs ropes suspended over a membrane pore were loaded at the center of their span through an AFM, which allowed to record both the applied load and the corresponding sample deflection, as shown in figure 2, (corresponding to 1999). Here it must be noted that authors considered SWCNTs ropes as an anisotropic beam rather than an ensemble of independent tubes. Elastic and shear moduli of SWCNTs ropes (dimeters ranging ~3–20 nm) were determined considering 200 nm lengths of ropes, assuming both ends clamped to the edge of the 200 nm pores of the substrate. The elastic and shear moduli were estimated to be ~1 TPa and ~1 GPa, respectively. Authors also reported on unexpectedly low inter-tube shear stiffness, as compared to reports on MWCNTs. This can be explained by the nature of shell-shell interaction. Ropes are generally made of twisted or tightly stacked individual SWCNTs whereas multiwall tubes generally represent concentric tubules arranged in a 'russian-doll' style stacking, one inside another. Additionally, post growth purification processing and specimen preparation could also play a role in the nature of tube-tube interfaces, quality or their interaction strength. Later, SWCNTs were characterized through tensile tests. In this case [57], the sample was attached to the tip of AFM, which was on turn connected to a piezo actuator made of bonded piezo films, which was used as a flexure element to provide the force and displacement needed. The AFM probe was used to pick up and isolate an individual SWCNTs rope from the 'SWCNTs- paper' for tensile testing, during which it also acted as the force sensor to read out the applied load, as shown in figure 2, (corresponding to 2000). Stress values were derived considering that the load was carried by the SWCNTs on the perimeter. Approximately half of the ropes broke at ~5.3% strain or lower, with an average breaking strength in the range of 13–52 GPa. Using the same model authors determined the average Young's modulus from 8 specimens in the range of 320–1470 GPa. Here the cross-sectional shape of the CNTs ropes was assumed circular (i.e. round) with

closed- packed array assembly, it was also assumed that all individual CNTs in the ropes were (10, 10) with an average diameter of 1.36 nm. More recently, in 2010, Wang *et al* presented experimental studies of direct measurements of tensile strength of SWCNTs using *in situ* HRTEM equipped with an AFM unit [58]. SWCNT regions (average length of such segments were ~100 nm, and diameters ranging from 1.3 to 5.4 nm) to be tested were derived from the consecutive inner wall breakdown/burning of MWCNTs. Analysis showed that the fracture strength varied in the range of 25 GPa to 100 GPa and these results were consistent with observation of morphology and structure differences. More uniform pristine SWCNTs observed in HRTEM before loading measured highest fracture strengths, and correspondingly a significant strength reduction was attributed by authors to the presence of visible structural defects, and other morphological imperfection. Additionally, authors noted that the irradiation-induced high-density defects also further reduced the strength, whereas the electrically-assisted annealing suppressed the formation of such defects.

Still based on AFM was the technique adopted to characterize nanowires vertically aligned from a growth substrate. In this case, the AFM tip was used to apply a transversal load along the length of the nanowire. The elastic properties, such as the strength and Young's modulus, were derived from the applied load and displacement (measured via AFM) and in conjunction with simple models derived from classical beam theory that were then refined through the Finite Elements (FE) simulations. Through such technique, the elastic modulus of ZnO nanowires with an average diameter of 45 nm was measured as equal to 29 $\pm$ 8 GPa [39]. In this case, AFM was used in contact mode using constant force regime and recorded lateral force responses (LFM signal) in order to perform elastic measurements on individual ZnO NW. To ensure that AFM tip is contacting and measuring one individual NW low density vertically aligned wires were studied, and the bending strength of silicon nanowires with a diameter of 90–170 nm resulted to be 12 $\pm$ 8 GPa [34]. It must be noted that these experiments are more straightforward, as they require less sample manipulation and offer the possibility to perform a number of tests in a single AFM scan, across many nanowires.

The bending configuration similar to those of the AFM experiments was recently adopted for the mechanical characterization of diamond nanoneedles [4]. In this case, the load and displacement delivered to the nanosample were applied and recorded by the means of a nanoindenter. This latter moved downward toward a single nanoneedle, and given the pyramidal shape of the nanoindenter tip, such movement resulted into a bending load applied to the nanoneedle itself. Such experiment revealed a surprisingly high elastic deformation capability (up to 9%) of diamond at the nanoscale, with a corresponding tensile strength in the range ~89–98 GPa [4].

2.2.1. MEMS testing platforms

The advent of MEMS gave further impulse to the experimental mechanical investigation of nanowires and nanotubes, as they provided miniaturized testing stages with load and displacement resolution, which nowadays can be as high as 0.2–0.4 μN and 1 nm, respectively, owing to their compatibility with electron microscopes (SEM/TEM) or high-resolution nanoindentation systems. Since mid-2000s, the literature has offered reports describing a wide variety of custom-made designs, which include small-scale platforms provided with all the actuating and sensing components needed to apply/sense the load and displacement delivered to a nanoscale sample under a tensile test, as shown in figure 2, (corresponding to 2007). Different actuation principles have been considered, such as thermal (single V-shaped actuator [75] or cascade V-shaped actuators [76]) or electrostatic actuation. Similarly, different load sensing strategies have been applied. In some cases, the load was measured electrostatically through capacitive sensors or optically through image processing of the deformation of an elastic element (with calibrated elastic constant). More technical details about the implementation of different actuating/load sensing strategies in MEMS testing platforms can be found in topical reviews [25, 77]. Starting from the 2010s, it is then possible to find, in addition to custom-made MEMS testing platforms, commercially available stages, such as the Push-To-Pull microfabricated devices developed by Hysitron (Bruker) (corresponding to 2011 in figure 2). Such device includes a MEMS platform, furnished with properly shaped springs and operated *in situ* SEM/TEM, that converts picoindenter delivered compression into a tensile force applied to the sample. The picoindenter then records both the applied load and displacement.

Such system was adopted to study the mechanics of different materials, including vanadium dioxide (VO_2) [72] and silver nanowires [78]. Tests on VO_2 nanowires revealed a stress plateau between about 0.48% and 0.75% strain, which corresponds to a phase transition induced by the uniaxial loading. From the slope of the stress-strain curve before and after the plateau, it was then possible to estimate the elastic modulus characterizing both monoclinic phases, which resulted to be 128 $\pm$ 10 GPa and 156 $\pm$ 10 GPa, respectively. Regarding silver nanowires, from the tensile tests, a ductile-to-brittle transition emerged when the diameter decreased below 100 nm, which was ascribed to the effect of the geometry confinement on dislocations activity.

Especially, quasi-static tensile tests have been reported, but in addition to them, there have been MEMS testing platforms developed to study the time-dependent mechanical response of nanowires under uniaxial testing [79] or under bending [45] (figures 3(a)–(b)). In this case, after a holding time during which a nanowire

was kept bended, its strain-recovery process was followed in real-time. Experiments performed on ZnO or p-doped Si nanowires revealed an anelastic behavior governed by Gorsky relaxation (i.e., relaxation associated to the motion of point defects in a non-homogeneous stress field), associated with an anelastic strain value up to four orders of magnitude larger than what previously observed at the macroscale [45].

Because of their electro-mechanical nature, MEMS mechanical testing platforms can also be enriched with additional functionalities, such as electrical contacts for the performance of electro-mechanical tests for the measurement of, for example, piezoelectric properties of 1D nanomaterials [73] as shown in figure 2 (corresponding to 2011). More generally, because of their design versatility, MEMS testing devices can be coupled with other physical characterization instruments in order to perform multi-physics analysis, such as strain engineering studies [25] or environmental mechanical studies aimed at investigating the mechanical behavior of materials in non-ideal (e.g., corrosive, redox, etc) environments, with these latter being a frontier of *in situ* nanomechanical studies [80]. Finally, temperature-dependent mechanical tests are also possible by developing a MEMS tensile testing platform compatible with SEM and cryogenic cell. Such setup was adopted, for example, in [49] in order to measure the surface dislocation nucleation strengths of ⟨110⟩ Pd highly crystalline nanowhiskers. *In situ* tensile test over a wide temperature range revealed a strong temperature dependence of strength, with this latter being reduced of nearly 6 GPa moving from 100 K to 450 K [49], thus suggesting thermal fluctuations playing a major role in surface dislocation nucleation.

Regarding the materials investigated via MEMS-based tensile testing stages, a wide variety of 1D nanostructures have been studied, including carbon nanotubes, semiconductor and metallic nanowires. For example, ZnO nanowires showed a remarkable dependence of the Young's modulus on their diameter (from 25–140 nm) [40] (figure 3(c)), supported also by computational fits. Gallium nitride (GaN) nanowires showed exceptional strength (4.0 $\pm$ 1.7 to 7.5 $\pm$ 3.4 GPa) and deformation capability (1 $\pm$ 1 to 4.2 $\pm$ 1.1% strain to failure) for a typically considered brittle material [41]. Failure modes reported in this study included clamp failure, transverse (nanowire c-plane) fractures, and insufficient force from the MEMS test actuator. Similar failures are frequently seen in other measured NWs especially when specimen diameters are ranging from ~100 to 200 nm. Body-centered cubic Nb nanowires revealed a superior plastic deformation capability (with a reported strain at failure of ~269%), which originated from a series of consecutively nucleated multiple reorientation processes and three distinct mechanisms, they characterized as, stress-activated phase transformation, deformation twinning, and slip-induced crystal rotation [46]. Single-crystalline Pd nanowhiskers showed linear elastic behavior up to 1% strain and clear non-linear behavior at larger strain [69]. Interestingly, in this case, one- and third- order elastic moduli, E and D, resulted to be size-dependent, while their slope, D/E, known as strain-expanded nonlinearity parameter, did not [69]. Phosphorous-doped silicon nanowires showed a Young's modulus of 170.0 $\pm$ 2.4 GPa [42] and a tensile strength of at least 4.2 GPa, while Si [100] nanowires fabricated from electroless etching showed a tensile strength of 5.4 GPa [42]. The fracture strength of silicon carbide (SiC) nanowires showed size effect, with nanowires of 17 nm diameter (25.3 GPa measured strength) approaching the theoretical strength value (28.5 GPa) of pure face-centered cubic SiC [43] (figure 3(d)). The observed size effect was mainly attributed to a size-dependent defect density more than surface effect. On the contrary, no clear size effect was instead observed for the Young's modulus. Silver nanowires resulted to have size dependent plasticity, with thinner nanowires showing an increasing number of local plastic zones formation, which provided higher fracture strain (up to ~14%) and strength (up to ~6 GPa) [47]. Tin oxide (SnO_2) nanowires with diameter of hundreds of nanometers were studied as possible lithium-ion battery anode materials. These were shown to possess fracture strength and Young's modulus of 2.53 $\pm$ 0.66 GPa and 91.74 $\pm$ 22.78 GPa, respectively, which however could be significantly decreased by lithiation-delithiation processes [44]. Highly deformable polymeric nanofibers, such as polyacrylonitrile (PAN) nanofibers, were also studied with custom-made MEMS platforms [81], resulting in 7.6 $\pm$ 1.5 GPa elastic modulus and large irreversible strains exceeding 220%, which was accompanied by cascade necking events. MEMS-based devices were also employed to study the mechanical properties of MWCNTs, both pristine and nitrogen-doped [48]. It was found that while the strength of pristine and nitrogen-doped MWCNTs was very similar (2.09 GPa versus 1.52 GPa, respectively), their behavior at higher stress was completely different, with pristine MWCNTs showing a linear elastic behavior up to fracture and nitrogen-doped MWCNTs showing varying degrees of nonlinearity [48]. Intershell-crosslinking increased the load-bearing ability for pristine MWCNTs (especially those comprised of ~100 shells), while in nitrogen-doped bamboo-like MWCNTs analyses of fractured specimens revealed a certain degree of plastic behavior before failure, as compared to pristine MWNTs that failed mostly via brittle bond-breaking. Authors concluded that such plasticity in CVD grown n-doped MWNTs which have shown kinks near the breakage points likely can be explained by a movement of kinks, which were formed/catalyzed during the growth.

Very recently, a custom-made MEMS tensile testing device, equipped with an electrostatic actuator and calibrated load sensing beams, was employed to determine the strength of structure-defined SWCNTs with initial length of ~5 μm [59], providing strength values overall in good agreement with previous results [58]

(figure 3(e)). Analyses of the measurements showed that near armchair, small diameter SWCNTs exhibited the highest tensile strength (figure 3(f)).

3. Two-dimensional nanomaterials (single or few atomic layer films, ultra-thin membranes) and their mechanical characterization

Soon after the discovery of graphene using scotch tape method, many 2D layered van der Waals materials followed, those include insulating hexagonal boron nitride (hBN), and semiconducting transition metal dichalcogenides (TMDs), such as molybdenum disulfide (MoS_2), tungsten disulfide (WS_2), tungsten diselenide (WSe_2) and many others. Given the fact that 'scotch tape' exfoliated graphene was declared not very practical for applications, although rendered the highest quality crystals, growth methods such as chemical liquid exfoliation which produced suspensions of graphene flakes or graphene oxide (GO), and catalytic chemical vapor deposition, providing selective growth on catalytic substrates, have been developed for production of large area single or few layered films. Reduced graphene oxide (rGO) and multi-domain (polycrystalline) single layered graphene have been successfully realized. Moreover the parameter field of other 2D materials also grew very fast [82, 83] in the recent years. In spite of the sharp increase in methods of fabrication of 2D materials, mechanical characterization of these materials has been proven challenging. In the next section we will describe most representative examples of 2D materials which have been synthesized and mechanically measured.

Studies reporting the mechanical characterization of 2D nanomaterials are relatively young, with the first experimental data about the Young's modulus of graphene dating back to 2007 [84]. As compared to 1D nanostructures, the manipulation of atomically thin films poses additional challenges, which have limited a widespread diffusion of the tensile testing stages previously developed for the mechanical characterization of nanotubes and nanowires. Conversely, other metrological strategies, mainly based on AFM, have been used more extensively.

3.1. Growth methods and synthesis techniques of 2D nanomaterials

Although 'scotch tape' exfoliation method of 2D materials preparation is still very popular and has been used in several studies of mechanical properties [6] more recently other methods, such as CVD, have also been utilized to fabricate specimens of 2D flakes or films for mechanical characterization which is governed by a need for larger scale (size) of 2D individual flakes or samples/specimens. Presently several leading methods exist to produce quality 2D specimens. Much alike 1D nanowires and nanorods, the solutions based methods of chemical exfoliation and drop casting of 2D flakes from liquid suspensions onto desirable surface or a mechanical device has been often used. In addition, the CVD grown 2D materials prepared on catalytic surfaces and transferred into desirable devices predominately via wet transfer process involving polymethyl metacrylate (PMMA), or polymethylsiloxane (PDMS) or other alternative methods are also often used. While each of these common methods of 2D materials production has its advantages, they also hav e specific differences. For example, to date the best quality 2D flakes come from scotch tape exfoliation of natural mineral crystal, such as graphene and other 2D materials, however, while graphite is an abundant material other 2D materials are not as commonly found in nature, hence need to be synthetically grown.

This places variety of CVD methods into a very desirable category of tools that allow for the development and production of large number of quality crystalline novel designed 2D materials from elemental precursor compounds. Several recent review articles focused on 2D materials synthesis could be useful for the reader [85, 86].

3.1.1. Graphene or graphene-like 2D nanomaterials

The CVD of graphene and hBN, for instance, can produce films of any desirable size, including large area, being constrained only by the geometry of the host substrate and size of the CVD chambers. As for single layered graphene and hBN the copper surfaces (single crystal or copper foils), are more often used, due to materials self-terminating properties. Other metal surfaces such as Ni, Ru, Pt and Pd have also shown to facilitate the growth, where the highest quality 2D materials have been shown to be synthesized also on single crystal metal surface, or epitaxial films [82, 83].

One remarkable difference between 1D and 2D nanomaterials preparation specifically for mechanical studies is that while 1D nanowires are now most commonly studied via *in situ* SEM using probe manipulators, 2D materials are quite difficult to study this way. Instead AFM based methods have gained significant popularity because it is relatively simple to prepare trenched substrates with scotch tape deposited 2D flakes atop and to study them using AFM indenter tips.

Indeed, first single layered graphene (SLG) membrane was measured by Lee *et al* [6], using 'scotch tape' exfoliated graphene flakes, mechanically deposited onto Si/SiO_2 substrate with prefabricated arrays of circular

holes etched in the substrate so that SLG flakes are overlaying the holes and therefore effectively suspended; those were identified using Raman characterization and subsequently tested for mechanical strength using AFM.

Another study by Lee *et al* [87], on suspended polycrystalline CVD grown SLG graphene membranes showed almost identical elastic stiffness to pristine graphene despite the grain boundaries which are normally present in polycrystalline graphene membranes. Authors reported on a slightly reduced strength in CVD-grown graphene as compared to exfoliated pristine flakes. In Lee *et al*, suspended specimens were prepared as follows: graphene was CVD grown on copper foils, the copper was etched with ammonium persulfate instead of $FeCl_3$, and PDMS was used to support the graphene during copper etching and to drystamp it onto the substrate without baking. Specimens were then transferred onto similar array of 1 to 1.5 μm diameter circular trenches and similar AFM indentation approach was used in mechanical characterization.

Wang *et al* [88], prepared their SLG by etching cosmetically samples of copper foils with CVD grown graphene purchased from *Graphenia LLC.* Samples where then pre-etched using ammonium persulfate (APS-100, Transcene) for 3−5 min to remove the graphene. Graphene was directly transferred onto etched-polycarbonate-membrane (PCTEM, Sterlitech) with various pore diameters. The residual copper foil was subsequently etched further by ammonium persulfate and the graphene/PCTEM composite was rinsed 3−5 times in deionized water (DI). Before drying, ethanol was mixed into DI to reduce the surface tension of the liquid to minimize potential damage. Burst tests to directly measure the burst pressures of graphene micromembranes were employed and SEM/AFM methods were used for imaging before and after. It was noted by authors that distribution of results highly depended on areas affected by wrinkles, which normally are often found in the CVD grown and transferred graphene.

In a new study Zhang *et al* [89], measured the fracture toughness of a CVD grown graphene using tensile testing of suspended graphene using a nanomechanical device *in situ* SEM. Specimens were prepared via dry transfer method as follows: the as-grown graphene on copper foil was first coated by PMMA and then attached to a PDMS block. The PDMS block had an open window slightly larger than the sample stage in the center. The PDMS/PMMA/graphene block was picked up from the etchant after copper was etched away in several hours, and transferred directly onto the stage. The stage was then covered by the PMMA/graphene film in the central window of the PDMS block. Heat treatment enabled the PMMA/graphene film to adhere to the suspended Si layer of the device smoothly and tightly. After calcining in air at 320 °C to decompose PMMA, a suspended film of graphene was obtained across the stage.

Several other investigations of mechanical properties were done on graphene and graphene oxide.

Regarding sample preparation for MEMS mechanical tests, Pérez-Garza *et al* [90] used mechanically exfoliated graphene, first prepared on SiO_2, then sample was covered with hydrophobic polymer and pulled off transferring graphene with it. Polymer/graphene stack was then floated in water bath, where it came in contact with prefabricated MEMS device once water was all pumped out carefully. In the final step polymer was dissolved releasing graphene flake onto MEMS device in a free standing form bridging the shuttles of the device.

Cao *et al* [91] measured mechanical strength of graphene oxide single layer membrane. GO was deposited from liquid suspension (prepared via chemical exfoliation of graphite) onto Si_3N_4 TEM grid with 2.5 μm holes and used AFM cantilever indentation approach for mechanical characterization in a similar fashion to that developed by Lee *at al* [6].

Aside from graphene and graphene oxide, other 2D materials have also been prepared and mechanically tested. These include hexagonal boron nitride (hBN), as well as some TMDCs. Being a close cousin to graphene in terms of hexagonal crystal structure and closely matched lattice constants, hBN has been considered a rival to the graphene and its unprecedented reported mechanical strength. Because of its insulating electronic properties hBN has unique standing in the world on 2D layered materials. In a study reported by Falin *et al* [92], authors described mechanical properties of hBN. Specimens of hBN mechanically exfoliated single and few layer crystals were placed on Si/SiO_2 substrates with pre-fabricated micro-wells of 650 nm diameter for subsequent measurements in AFM by indentation at the center of the suspended regions.

3.1.2. Transition metal dichalcogenides (TMDC) 2D nanomaterials

The 2D van der Waals materials such as transition metal dichalcogenides have also been studied mechanically. Many of single layered TMDCs are direct band gap semiconductors with a remarkable optical sensitivity and expected high in-plane mechanical strength. Few studies on MoS_2 and WS_2 mechanical properties have been reported [93–95]. Bertolazzi *et al* [93] and Liu *et al* [95] measured breaking strength of single and few layer MoS_2, where flakes of MoS_2 were prepared using mechanical exfoliation of MoS_2 crystal and CVD respectively. In the studies by Bertolazzi *et al* and Liu *et al* flakes were prepared in a similar fashion, mounted on Si/SiO_2 substrate containing micro-fabricated circular holes with ~550 nm to 1 μm diameter). Liu *et al*, used PDMS stamping to transfer flakes from host growth substrate into a holey Si/SiO_2 for subsequent measurements of elastic moduli of 2D layers through AFM nanoindentation. Lastly Castellanos-Gomez *et al* [94] measured mechanical properties

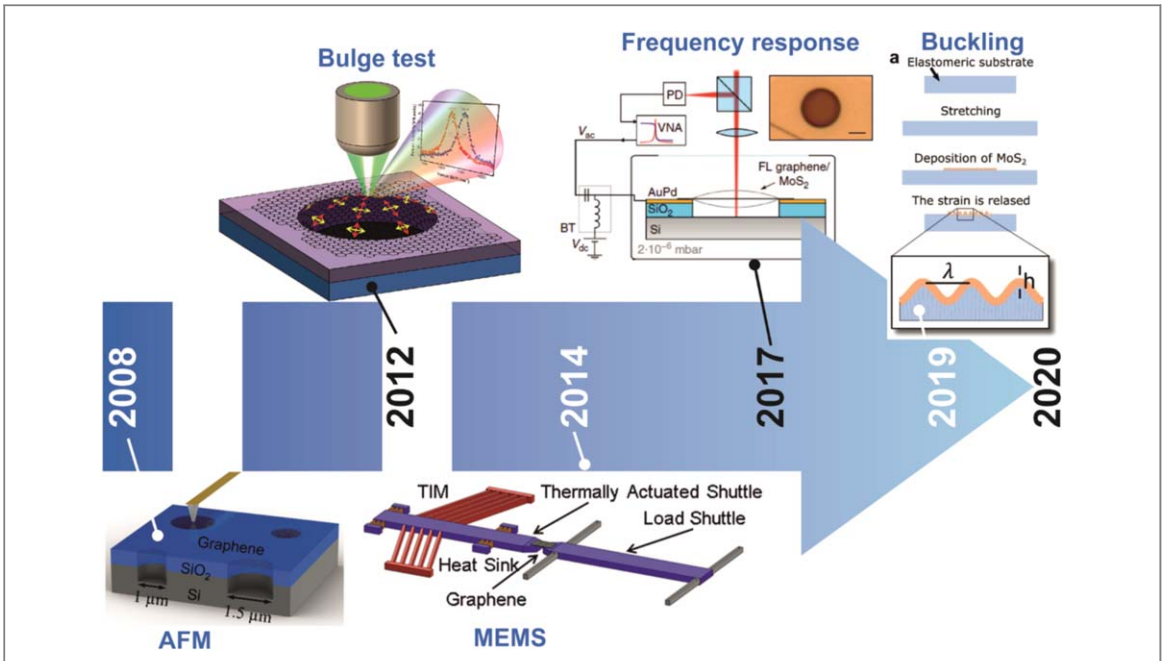

Figure 4. Overview of the different mechanical characterization approaches adopted for 2D nanomaterials since 2008 and their temporal evolution. The first characterization method reported for an atomically thin material (graphene in this case) was based on the deflection of a freestanding membrane loaded at the center with an AFM tip [6] (Reprinted with permission from [98]. Copyright 2016, American Chemical Society); later a bulge test combined with Raman spectroscopy was proposed in order to derive the Young's modulus of graphene [99] (Reprinted with permission from [99]. Copyright 2012, American Chemical Society); in 2014 the first MEMS platform was reported, capable of applying uniaxial strain >10% to graphene nanosheets [100] (Reprinted with permission from [100]. Copyright 2014, American Chemical Society). In 2017, a novel method based on the detection of the frequency response of 2D nanomaterial drums was proposed in order to derive their Young's modulus [101] (Reprinted under the terms of the Creative Commons CC BY license from [101]. Copyright 2017, Springer Nature). In 2019, there was a revival of high-throughput buckling-based technique (first appeared few years ago [102]) allowing to derive the Young's modulus of 2D nanomaterials from the detection of the rippling wavelength induced in the nanofilm by the stress release of a pre-stretched polymeric substrate [103] (Reprinted with permission from [103]. Copyright 2019, Wiley-VCH Verlag GmbH & Co.).

of multilayer MoS_2 from 20 layers down to 5 layers. Flakes/specimens were transfered from MoS_2 natural crystal via PDMS stamping directly into ~1.1 μm diameter holes and 200 nm deep ecthed-in tranches.

Studies of WSe_2 and $MoSe_2$ mechanical properties were reported by Zhang *et al* [96], and Yang *et al* [97], respectively. Exfoliated from bulk crystal, (supplied by 2D Semiconductors Inc.), multilayer WSe_2 flakes were prepared in a similar fashion using mechanical transfer process for subsequent measurements of their elastic properties using established AFM indentation strategies. Flakes were transferred onto a sample with circular holes etched in Si/SiO_2 substrate (diameters ranging ~1.6–2.6 μm) using PDMS stamps. Studies reported by Yang *et al* [97] show large area $MoSe_2$ synthesized by CVD. Single and few layer flakes were identified prior to transfer. Transfer from growth substrate onto nanomechanical device was performed in a sequential multi-step process. Sample with flakes was coated by PMMA, then Si/SiO_2 was etched in NaOH solution where $PMMA/MoSe_2$ stack was released and subsequently fished-out using Cu TEM grid. Next, the specimen was manipulated and picked up by a probe from Cu grid and placed $PMMA/MoSe_2$ stack directly onto the nanomechanical device, PMMA was removed via heat treatment. FIB was employed to cut specimen into desirable shape prior to measurements.

3.2. Overview of the testing platforms for mechanical characterization of 2D materials

Over the years, different strategies (figure 4) have been adopted for the mechanical characterization of a variety 2D nanomaterials (figure 5). These can be categorized as: AFM nanoindentation, bulge test, membrane deflection test, resonance test, buckling metrology or MEMS-based tensile test; each of them allows to derive different information about the mechanical behavior of tested materials (table 1).

Historically speaking, the first and currently most popular technique is based on AFM nanoindentation.

In this configuration, the AFM tip applies an increasing force at the center of a freestanding 2D material membrane and simultaneously records both the load and the deflection delivered to the sample, as shown in figure 4 (corresponding to 2008). Such data are then introduced into models derived from thin plate theory, assuming nonlinear elastic stress-strain response, in order to extrapolate the strength, the strain at fracture and the Young's modulus of the tested sample [6, 105]. This testing configuration was applied to single layered graphene [6], which resulted in an extracted value of Young's modulus of 1 TPa, and strength and fracture strain

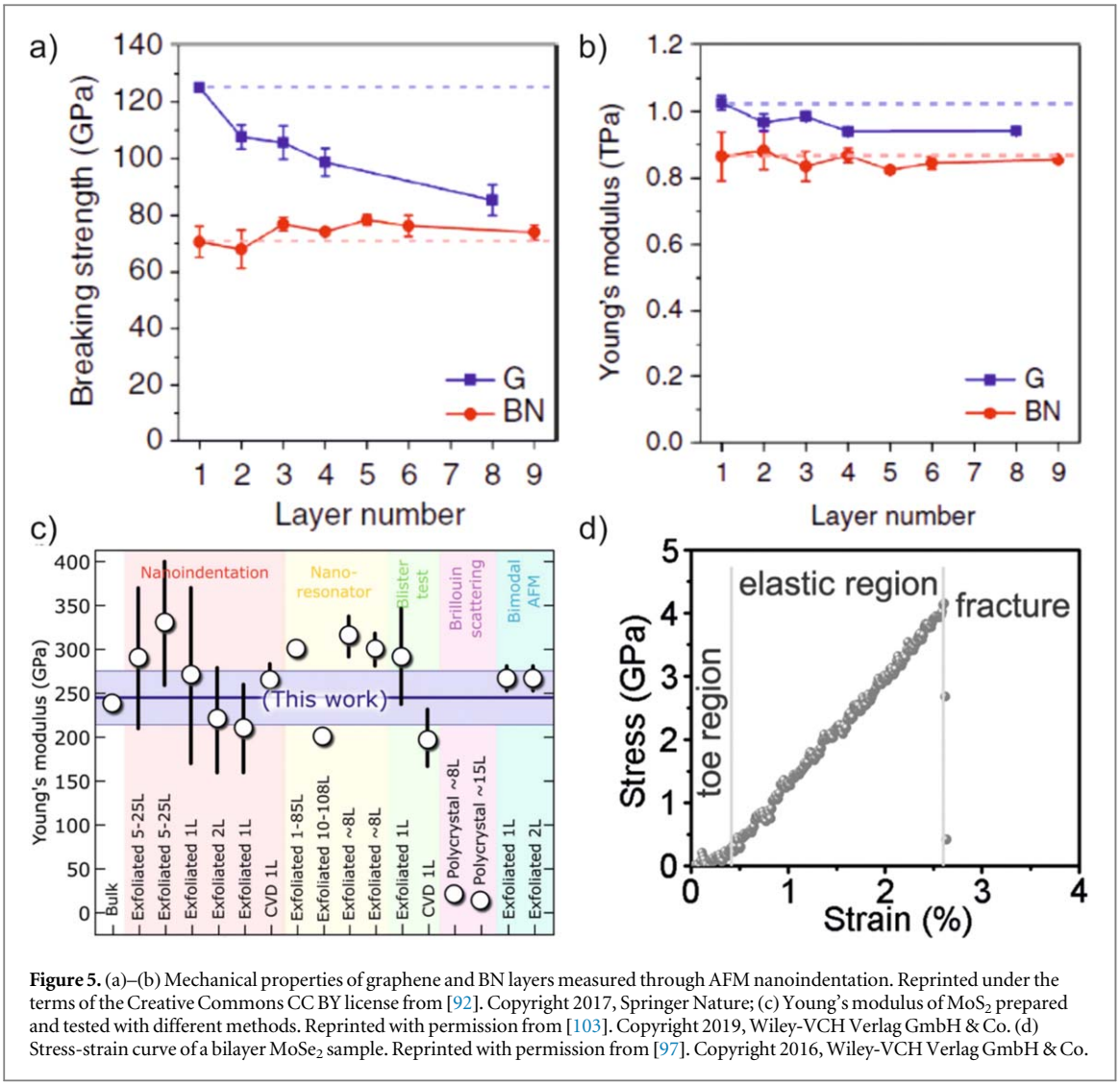

Figure 5. (a)–(b) Mechanical properties of graphene and BN layers measured through AFM nanoindentation. Reprinted under the terms of the Creative Commons CC BY license from [92]. Copyright 2017, Springer Nature; (c) Young's modulus of MoS_2 prepared and tested with different methods. Reprinted with permission from [103]. Copyright 2019, Wiley-VCH Verlag GmbH & Co. (d) Stress-strain curve of a bilayer $MoSe_2$ sample. Reprinted with permission from [97]. Copyright 2016, Wiley-VCH Verlag GmbH & Co.

Table 1. Mechanical properties of 2D nanomaterials that can be derived by different mechanical characterization methods.

Testing strategy	Mechanical properties
AFM nanoindentation	Young's modulus [6], strength [6], strain to failure [6]
Bulge test	Adhesion energy [36], Young's modulus [99]
Membrane deflection test	Young's modulus [104]
Resonance test	Young's modulus [101]
Buckling metrology	Young's modulus [103]
MEMS-based tensile test	Full stress-strain curve [97]

of 130 GPa and 25%, respectively. With a similar testing configuration, it was possible to evaluate how mechanical properties are affected by induced defects [106]. In particular, it was found that while the elastic modulus is almost insensitive and the strength slightly (~14%) affected by defect density in the sp^3-type defective regime, in the vacancy defective regime both mechanical properties significantly reduce. AFM nanoindentation tests were also carried out on polycrystalline graphene and demonstrated that the presence of grain boundaries does not affect its stiffness and strength [87]. Graphene oxide monolayers with high carbon-to-oxygen ratio (~4:1) resulted in a Young's modulus of 384 ± 31 GPa and strength of 24.7 ± 4.5 GPa [91]. Graphene oxide membranes revealed to be a powerful platform to investigate mechanochemical transformations due to strain [107]. In particular, it was showed that as a consequence of the applied mechanical load, epoxide-to-ether transformation occurred, providing GO membranes, functionalized with cyclic epoxide groups, with a ductile behavior. Beyond graphene-based materials, also other 2D materials were tested through AFM

nanoindentation. For example, BN nanosheets were investigated to derive their strength, Young's modulus and fracture strain [92], which, in the case of monolayers, resulted to be 70.5 ± 5.5 GPa, 0.865 ± 0.073 TPa and 12.5 ± 3.0%, respectively (figures 5(a), (b)). In contrast to graphene, no significant change of fracture strength in single versus few layered hBN, was observed which contrasts with the graphene fracture strength which diminished significantly with the increasing number of layers (about ~30% from 1 layer to 8 layers i.e. close to bulk). This difference was attributed to the distinct interlayer interactions between adjacent graphene layers as compared to BN layers.

Regarding transition metal dichalcogenides, both MoS_2 [93–95], WS_2 [95] and WSe_2 [96] were investigated. From such experiments, MoS_2 showed a Young's modulus of 270 ± 100 GPa [93], a strain at break in the range of 6%–11% [93] and a strength of 22 ± 4 GPa [93] (figure 5(c)). WS_2 showed similar elastic properties, with a reported Young's modulus of 272 ± 18 GPa, while WSe_2 was derived to be less stiff, with a Young's modulus of 167.3 ± 66.7 GPa, with such value not statistically affected by the number of atomic layers.

As in AFM nanoindentation tests, bulge tests (known also as pressurized blister tests) require the availability of a free-standing membrane, which is usually obtained from the deposition of a relatively large 2D nanomaterial flake over a perforated substrate. Compared to AFM nanoindentation, load is applied through a pressure difference between the upper and the lower surface of the membrane, which avoids onset of stress concentration [108]. Owing to its gas impermeability [109], graphene can sustain a pressure difference of several bars [88]. As the pressure difference increases, the membrane, which is clamped along its periphery by Van der Waals forces, deflects by an amount depending on the applied pressure difference, the film thickness, the Poisson's ratio and the Young's modulus, which can then be extracted through fitting an analytical model available from continuum mechanics [108]. The sample deflection can be measured through AFM, as in [36], where the adhesion energy between monolayer graphene and SiO_2 was also derived. In this case, the pressure difference was increased until the graphene membrane detached from its SiO_2 substrate. The bulge test configuration can also be coupled with Raman spectroscopy [99] instead of AFM in order to derive the actual strain applied to the sample, as shown in figure 4 (corresponding to 2012). Indeed, Raman spectroscopy revealed to be a rich and indispensable tool for the characterization of graphene and other 2D nanomaterials. The peculiar G and 2D peaks that characterize graphene are extremely sensitive to a variety of external and internal factors, such as an applied mechanical strain [110]. For example, the shifts of the Raman G and 2D peaks were recorded and then converted into a measurement of the biaxial strain applied to a graphene monolayer suspended over a microcavity inserted into a pressurized chamber. Such strain values were compared to the results of numerical simulations reproducing the same experimental configuration, in order to end up with an estimation of the Young's modulus (2.4 ± 0.4 TPa [99]). It was noted by authors that distribution of results highly depended on areas affected by wrinkles, which normally are often found in the CVD grown and transferred graphene [88].

In analogy to the bulge test is another non-contact technique, the membrane deflection test, where the 2D material sample is still in the shape of a freestanding circular membrane clamped at its periphery to a pre-patterned silicon nitride (Si_3N_4) substrate. The membrane is deflected by the electrostatic force originating from a voltage applied between the membrane itself and a bottom electrode. The sample displacement field is acquired through interferometric profilometry [104]. Through this testing configuration, the in-plane stiffness of graphene, was extracted from an analytical model relating the applied pressure, the deflection at middle membrane, the radius of the sample membrane, in the temperature range of 4–400 K, showing that graphene softening at temperatures $<$400 K can be mainly ascribed to its static wrinkling.

Similarly, based on the electrostatic actuation of a freestanding membrane biased with respect to a bottom electrode is the resonance technique recently proposed in [101], as shown in figure 4 (corresponding to 2017). In this case, the non-linear frequency response of the membrane was acquired and then fitted in order to derive its Young's modulus and its pre-stress value. The membrane displacement was recorded by laser interferometry that was proven to guarantee high resolution capability. Through this configuration, both graphene and MoS_2 circular nanodrums of few nanometers thickness were tested and their elastic modulus resulted to be 594 ± 45 GPa and 315 ± 23 GPa, respectively.

All the testing schemes presented up to now require the nanomaterial sample to take the shape of a freestanding membrane. Even though established routes are now available for the transfer of atomic thin layers from the native to target substrates, the preparation of pre-patterned substrates for 2D materials membrane suspension and probing/actuation involve microfabrication and technically demanding experimental setups. In this regard, a valid alternative technique was recently proposed for evaluating the Young's modulus of a variety 2D nanomaterials [103]. This technique is based on the buckling metrology developed few years ago for polymeric films with thickness in the range of nano/micrometers [102]. According to such testing method, the ultra-thin film under investigation was transferred on a pre-stretched polymeric substrate. When the substrate strain was released, the film resulted to be under compression with the occurrence of a buckling instability, as shown in figure 4 (corresponding to 2019). The wavelength characterizing the buckling instability, which can be

detected by either optical inspection or AFM (if ripples with periodicity of ~200–300 nm and few nanometers amplitude have to be resolved), could be related via an analytical model to different system characteristics, including the thin film Young's modulus. For example, through this technique, the Young moduli of MoS_2, $MoSe_2$, WS_2 and WSe_2 were reported as 246 ± 35 GPa, 224 ± 41 GPa, 236 ± 65 GPa and 163 ± 39, respectively.

While different cyclic tests have been reported on 1D nanostructures, only limited data are available in the case of 2D materials. For example, AFM nanoindentation was shown as able to induce stiffening of graphene monolayers with the number of loading cycles [111] and evidence of hysteretic energy dissipation with recoverable interlayer slippage was reported in multi-layer graphene [98]. Very recently, again based on AFM nanoindentation, it was shown that graphene, in mono- and few-layer form, possesses a superior fatigue life; being able to survive more than 10^9 cycles under a mean stress of 71 GPa and stress range of 5.6 GPa [112]. In general, reported results about the fatigue behavior of 2D nanomaterials are still very rare.

3.2.1. MEMS testing platforms

Tensile tests are universally recognized as the most straightforward means to derive the majority of mechanical properties of materials, hence efforts have been devoted to the development of tensile testing stages compatible with 2D nanomaterials that enable in-plane loading in contrast to a transverse loading which is usually more common in AFM nanoindentation based measurements. Currently, only few examples have been reported in the literature [89, 90, 97, 100]. In the first case [90, 100], a typical stage comprising a thermal actuator and a capacitive load sensor was used to apply significant high strain (>10%) to graphene layers with variable thickness and to record the corresponding load (corresponding to 2014 in figure 4). Surprisingly, the Raman spectra that were acquired, as well, showed a significantly smaller shift of the characteristic graphene peaks than expected. It was suggested by other authors [113] that it was possible that reported (>10%) strain to graphene was not achieved in the experiment. In the second case [89, 97], the authors applied the nanomechanical device actuated by a nanoindenter operated *in situ* SEM, which was previously developed for tensile testing of 1D nanostructures [32]. Both the load and the displacement applied to the sample were measured through the nanoindenter itself. Such configuration was adopted to measure the fracture toughness of mostly graphene bilayers with controlled pre-cracks introduced by FIB [89], and to derive the stress-strain curve of $MoSe_2$ mono- and bilayers [97] (figure 5(d)).

In addition to custom-made platforms, as those described above, there are also examples of commercial testing devices applied to study the mechanical properties of 2D materials, such as the Push-to-Pull device by Hysitron, described in the previous section regarding 1D nanostructures. This was used to derive the fracture toughness of a graphene bilayer [114] and, very recently, to perform a tensile test on graphene monolayer, which showed a strength of 50–60 GPa, a Young's modulus of ~0.9–1 TPa and a strain at failure of up to ~6% [115] This same apparatus was also applied on amorphous oxide ultra-thin films of a-Al_2O_3, with a nominal thickness of about 40 nm, which fractured at 15% strain, with an associated plastic strain of 5%–8% [116].

Following the great successes that have already been demonstrated in the mechanical characterization of 1D nanostructures, it can be expected in the next several years a similar widespread proliferation of MEMS tensile testing platforms would occur to 2D nanomaterials, as well.

4. Discussion

With reference to the above mentioned mechanical characterization techniques, we can summarize that for 1D nanomaterials, it is clear that the manipulation and transfer of an individual NW from host growth substrate onto measuring devices as well as clamping/welding of the ends of the nanowire is a common strategy in mechanical measurements that are performed using MEMS devices or with other types of mechanical actuators, and it has been widely used by many researchers. Nevertheless, it is still considered to be a time consuming and labor intensive process, requiring sophisticated *in situ* high resolution imaging systems, such as SEM and TEM, regardless of the particulars of a specific MEMS platform employed for the measurement. On the other hand, AFM cantilever or nano-indenters and other piezo driven mechanical systems were also successfully implemented and used, which did not require removal of the nanowires, from the host growth substrates, although in this case predominately vertically oriented nanowires selectively prepared in low density forests can be effectively tested, to ensure the measurement of individual specimen. This approach could be considered less labor intensive, as no removal of the materials from the host growth substrate is needed. Nevertheless, it seems that majority of individual nanowires and nanotubes are characterized with *in situ* SEM using micromanipulators and direct imaging. Nowadays, most of the studies report mechanical characterization of 1D nanomaterials via tensile testing; however, applications in flexible or wearable electronics need a deep knowledge of 1D nanomaterials behavior under bending, as well [117, 118].

Table 2. Key features of representative mechanical testing methods and platforms for 1D and 2D nanomaterials.

	Specimen					
Testing strategy/ device	Topology	Material	Size	Loading configuration	Force measurement & resolution	Displacement measurement & resolution
Resonance	1D	MWCNT [71]	Length: 1–5 μm; inner diameter: 1–2 nm; outer diameter: 5.6–24.8 nm	Resonance induced by thermal vibration	Not measured	TEM imaging
		MW BNNT [37]	Diameter: 3.5 nm; length: 153. 8 nm		Not measured	TEM imaging
	2D	Graphene, MoS_2 [101]	Thickness: 5–8 nm; circular membranes with 2–2.5 μm diameter	Resonance induced by electrostatic actuation	Electrostatic actuation	Laser interferometry
AFM	1D	SWCNT ropes [56]	Diameter: 3–20 nm; length: 100–370 nm	Bending	AFM	AFM
	1D	SWCNT ropes [57]	Diameter: 20–41 nm; length: ~10 μm	Tensile	SEM imaging & calibrated AFM probe	SEM imaging
	1D	ZnO NW [39]	Diameter: 25–65 nm; length: 167.9–683.4 nm	Bending	AFM (cantilever stiffness: normal spring constant of 4.5 N m^{-1} and a lateral spring constant of 1378.1 N m^{-1})	AFM
	1D	Si NW [34]	Diameter: 90–190 nm; length: 500–2000 nm	Bending	AFM	SEM imaging
	2D	Single layer graphene [6]	Circular membranes with 1–1.5 μm diameter	Bending	AFM (accuracy of the force measurement: ±9.5%)	AFM (displacement accuracy: 3.2%)
	2D	Single layer graphene oxide [91]	Circular membranes with 2.5 μm diameter	Bending	AFM (cantilever stiffness: 34.2 N m^{-1})	AFM
	2D	BN, Graphene [92]	Thickness: G:1–8 layers; BN: 1–9 layers; circular membranes with 1.3 μm diameter	Bending	AFM	AFM
	2D	MoS_2 [93]	Thickness: 1–2 layers; circular membranes with 550 nm diameter	Bending	AFM (resolution: ~1 nN)	AFM
	2D	MoS_2 [94]	Thickness: 5–25 layers; circular membranes with 1.1 μm	Bending	AFM Cantilever stiffness: 0.88 N m^{-1})	AFM
	2D	MoS_2, WS_2 [95]	Thickness: 1 layer and bilayer heterostructures; circular membranes with 1.1 μm diameter	Bending	AFM Cantilever stiffness: 43.8 N m^{-1})	AFM
	2D	WSe_2 [96]	Thickness: 5–14 layers; circular membranes with 1.55 μm and 2.6 μm diameter	Bending	AFM (probe spring constant: 35.7 N m^{-1})	AFM
Bulge test	2D	Graphene [36]	Thickness: 1–5 layers; circular membranes with 5 and 7 μm diameter	Bending	Pressure variation	AFM
	2D	Graphene [99]	Thickness: 1–2 layer; circular membranes with 2.0–7.3 μm diameter	Bending	Pressure variation	Strain measured by Raman spectroscopy (spectral resolution: 0.7 cm^{-1})

Table 2. (Continued.)

Testing strategy/ device	Specimen			Loading configuration	Force measurement & resolution	Displacement measurement & resolution
	Topology	Material	Size			
Membrane deflection	2D	Graphene [104]	Thickness: 1 layer; circular membranes with 7.5–30 μm diameter	Bending	Electrostatic actuation (uncertainty in applied pressure is below 5% for all voltages)	Interferometric profilometry (sub-nanometer precision in the out-of-plane direction; sub-micrometer precision in the in-plane direction)
Buckling metrology	2D	MoS_2, $MoSe_2$, WS_2, WSe_2 [103]	Thickness: 3–11 layers; size: tens of μm	Buckling instability	No force measurement	Optical microscopy or AFM
Nanoindentation	1D	Diamond nanoniddles [4]	Diameter: 160–230 nm; length: few μm	Bending	Picoindenter (Force noise floor: <0.4 μN)	Picoindenter (Displacement noise floor: <1 nm)
Custom-made MEMS	1D	Ag [79]	Diameter: 68–95 nm; length: few μm	Tensile	Load applied by a thermal actuator; Voltage feedback control of a capacitive load sensor	SEM imaging (sub-nanometer)
	1D	ZnO NW [40]	Diameter: 20.4–412.9 nm; length: few μm	Tensile	Load applied by a thermal actuator; capacitive sensor with 11.8 nN- 12.2 μN resolution [75]	SEM imaging
	1D	GaN NW [41]	Diameter: 151–380 nm; length: 4.58–13.97 μm	Tensile	Load applied by thermal actuator; load measured by SEM imaging of pre-calibrated spring.	SEM imaging (resolution: 40–80 nm)
	1D	Si NW [42]	Diameter: 20–200 nm; length: 18 μm	Tensile	Electrostatic actuation; load measured by capacitive load sensor (resolution: 1 nm)	SEM imaging (resolution: 10 nm)
	1D	SiC NW [43]	Diameter: 26–42 nm; length: few μm	Tensile	Thermal actuation; capacitive load sensor (resolution: 12 nN)	SEM imaging (resolution of strain measurement: 0.03%)
	1D	SnO_2 NW [44]	Diameter 100–800 nm: length: 2867–15 424 nm	Tensile	Nanoindenter (resolution: $\sim$1 μN)	Nanoindenter (resolution 0.8675 nm)
	1D	MWCNTs [48]	Diameter: 70–100 nm; length: few μm			
	2D	Graphene [89]	Thickness: 1–2 layers; length: few μm; width: few tens μm			
	2D	$MoSe_2$ [97]	Thickness: 1–2 layers; length: 2666.7–6107.3 nm; width: 4776.0–16 034.1 nm			
	1D	PAN nanofibers [81]	Diameter: 300–600 nm; length: 25–50 μm	Tensile	Actuation by piezoelectric transducer; load measured via optical microscopy (resolution: $\sim$50 nN)	Optical microscopy (resolution: 50 nm)

Table 2. (Continued.)

Testing strategy/ device	Specimen			Loading configuration	Force measurement & resolution	Displacement measurement & resolution
	Topology	Material	Size			
	1D	SWCNTs [59]	Diameter: 0.61–3.03 nm; length: ~5 μm	Tensile	Electrostatic actuation; force measured by calibrated beams via SEM imaging	SEM imaging
	2D	Graphene [90, 100]	Thickness: 3 layers; length: 22.7 μm; width: ~10 μm	Tensile	Load applied by thermal actuator; load measured via optical tracking	Optical tracking
Commercial MEMS	1D	VO_2 NW [72]	Diameter: few hundreds nanometers; length: 7.8 μm	Tensile	Push-To-Pull MEMS actuated by Hysitron/Bruker Picoindenter (nominal resolution: <0.2–0.4 μN)	Push-To-Pull MEMS actuated by Hysitron/Bruker Picoindenter (nominal resolution: and <1 nm)
	1D	Ag NW [78]	Diameter: 50–300 nm; length: few μm			
	1D	Pd NW [49]	Diameter: 30–150 nm; length: ~2-~7 μm			
	2D	Graphene [114]	Thickness: 2 layers; width: 2.17 μm; length: 2.36 μm			
	2D	Graphene [115]	Thickness: 1 layer; width: 3.4 μm; length: ~3 μm			

From reported studies on 2D single and few layer materials such as graphene, GO, hBN, MoS_2, WS_2, $MoSe_2$ and WSe_2, one can summarize the sample preparation strategies as falling into couple of general categories: CVD growth or mechanically or chemically exfoliated from crystal.

Both, mechanically exfoliated or CVD grown 2D materials are studied most often using AFM nanoindentation strategies. This method is simple and does not require specimen manipulation, except when CVD grown samples are used. In this case, they generally need to be transferred from growth substrate into a clean surface with prefabricated holes using either PMMA based transfer or PDMS stamping. An alternative method reported involved custom built nanomechanical or micromechanical devices, where more intricate specimen manipulation is needed to precisely position 2D flake at the desired location in the device in the proximity of the shuttle area. This method of transfer and placement of specimen is more time consuming and labor intensive. Although individual studies employing these sample preparation tactics have successfully demonstrated capabilities of detailed mechanical characterization, testing and analysis of a number of 2D materials, still these methods lack standardization and generalization of the process flow that could be applicable for variety of other 2D materials and heterostructures.

In the following sections we will categorize methodologies by testing approaches (table 2), specifics of sample preparation and will highlight their advantages and the challenges that still persist in fabrication process and in testing. Different approaches which are being used often provide alternative routes to measurements and at the same time they also allow for additional complimentary data to be extracted and derived from the measurements.

4.1. Top-down approach

One of the main challenges related to the mechanical characterization of low dimensional nanoscale materials is related to the manipulation, alignment and gripping of nanosamples. While to mitigate misalignment issues, proper design strategies can be adopted [119], manipulation of externally grown nanospecimens and mounting them on the mechanical testing stages require complex, time consuming procedures. There are few main top down approaches to manipulate and position specimen on the mechanical stages depending on the size of the specimen: mainly manual positioning and manipulation [81], dielectrophoresis and robotic micro/nano-manipulators [120]. In case of manual placements, only relatively large size samples (diameter/length) can be successfully realized. With dielectrophoresis although easily scalable, contamination may frequently occur. The robotic manipulator tools offer much flexibility for handling of small size specimens with high precision and in controlled environment. However, this approach is not very scalable and an extreme care has to be taken when the nanosample is fixed at its ends to the testing platform; operation usually performed by EBID of inert material. Most of the time the strain measurement of the sample relies on the measurement of the relative displacement between the clamps, which have to be sufficiently stiff in order not to induce artifacts in the data analysis [121].

It is worth mentioning that the top-down strategies are also usually adopted for the mechanical characterization of 2D nanomaterials. Indeed, typically, 2D membranes are grown on catalytic substrates and then transferred onto the target substrates (either pre-patterned, as those for AFM nanoindentation [6] or MEMS-based platform [89], or onto the flexible substrates as in buckling-based methodology) integrated in the testing system [103].

4.2. Bottom-up approach

One way to overcome issues related to the manipulation of nanospecimens is the direct fabrication/growth of the nanomaterial of interest on the testing platform. For example, materials such as PDMS [122], gold [123], C_{60} [124], are compatible with standard lithography and allowed thin films to be successfully co-fabricated with MEMS tensile testing platforms. The range of printable nanomaterials continues to expand and recent progress in additive manufacturing (such as two-photon lithography) allowed to directly write on MEMS and subsequently test polymer micro/nanostructures over a wide range of geometries [125], including elemental building block, such as nanowires with cross-section as small as $200 \times 400\ nm^2$ [126]. Furthermore, other types of materials could be also produced via direct assembly and growth on microdevices. In particular, 3D biomimetic tissues were showed as able to self-assemble onto a MEMS tensile testing stage, which allowed to monitor the force generated during the growth of the tissue sample, as well as to derive its stress-strain curve [127].

Direct synthesis of 1D nanostructures at targeted location of Si platforms has also been reported [128]. In this regard, different approaches have been employed. For example, in the case of Si nanowires, their fabrication can be successfully integrated with the fabrication of MEMS tensile testing stages [129]. Focused ion beam was also used to deposit carbon nanowires directly on an electrostatic actuated nanotensile testing device from phenanthrene gas [130]. Alternatively, *in situ* TEM welding of two nanoscale crystals was implemented for direct

fabrication of bi-crystal nanowires onto a tensile testing platform [46]. Regarding bending tests through AFM approach, more examples are available of tests performed on single nanowires [34, 39]. We emphasize that to date no application of bottom-up mechanical characterization approaches have yet been reported for 2D nanomaterials.

4.3. Advantages and challenges

Technological advances in fabrication and manipulation of micro/nanocomponents have offered possibilities for improved positioning/mounting nanostructures, such as nanotubes and nanowires, on the target locations on miniaturized mechanical testing stages. This, in turn, boosted the development of MEMS based mechanical testing platforms especially by the late 2000s. One would have expected an extension of the experimental setups initially applied to 1D nanostructures also to 2D nanomaterials. However, the manipulation and transfer of ultra-thin films revealed to be significantly more challenging with a consequent limited number of tensile tests conducted onto atomically thin sheets. Additionally, most of the time laborious and time-consuming manipulation of nanoscale objects is still required when performing tests through MEMS testing devices.

Conversely, AFM based mechanical testing techniques may take advantage of well-assessed protocols now available for the sample preparation. Relatively large atomically thin membranes can be transferred onto a perforated substrate, which provides a number of locally suspended samples to be tested. This is one of the reasons behind the popularity of such AFM based techniques. However, even though high-resolution load and displacement measurements are readily available with the AFM based testing, there are certainly a number of parameters which are not always exactly defined or taken into account such as the tip radius and exact shape, the load position and gradient, and the presence of possible stress concentration. Further, the loading configuration is not ideal, as the applied stress state is biaxial [131] and a non-uniform strain field could be introduced in the 2D material sample by the local probing [27]. As a matter of fact, it was demonstrated by atomistic simulations that the strength of bilayer graphene, with grain boundaries with varying misorientation tilt angles, measured by AFM nanoindentation can deviate from the tensile strength by up to 50%, with the tendency of this latter to underestimate the pristine graphene strength and overestimate the polycrystalline graphene strength [132]. Apart from intrinsic errors in the extrapolation of quantitative data related to the application of models that were not originally derived for atomically thick materials [133], AFM nanoindentation also does not allow real-time imaging of the sample deformation; the possibility that is instead guaranteed by *in situ* SEM/TEM tensile testing platforms. To that end MEMS platforms can now provide high force and displacement resolution, such as the commercial device (e.g., PicoIndenter PI95) delivered on the market by Hysitron/Bruker Inc., which is provided with a nominal load noise floor of 200 nN, 1 mN maximum force, a nominal force and displacement resolution of <0.2 μN and <0.02 nm, respectively [49]. In addition to commercial solutions, MEMS devices can, in principle, be designed specifically to precisely apply and sense/measure nanoscale loads and displacements, such as the recently reported mechanical stage performance in [126] with impressive load and displacement resolution of 126 nN and 1.8 nm, respectively. A custom-made design evidently offers significant advantage by allowing to include additional desired functionalities, such as thermal management capability as reported in [134, 135], which here enabled tensile testing of 1D nanomaterials over the controlled and tunable temperature ranges. Such features are currently of great interest, as in many applications, including aerospace and automotive, nanomaterials are required to withstand combined thermal and mechanical loadings, and temperature can significantly affect their mechanical behavior. However, reports on mechanical characterization of 2D nanomaterials at non-ambient temperature are still rare. Real-time observation *in situ* SEM/TEM requires the nanostructure of interest to be exposed to electron beam, which can affect the sample itself causing contamination, charging, heating, etc, just to mention few possible side effects [136]. Another limit of MEMS-based testing platforms refers to their limited capability in capturing the plastic behavior of nanomaterials. Such limit stems from the relatively low frame stiffness of the testing platform, which cannot accommodate the substantial strain energy release that often accompanies the onset of plasticity in nanomaterials, such as metallic nanowires [137, 138]. In order to overcome such issue and perform tensile tests under true displacement control, alternative MEMS designs should be considered [139], which implement rigid frames [138] or electrostatic feedback-control able to prevent displacement of compliant structures, such as load sensor unit [140]. Many times, experimental studies on the mechanical behavior of nanostructures are accompanied by molecular dynamics (MD) simulations [141]. These, in fact, allow to achieve a deep understanding of the mechanisms responsible for the observed mechanical behavior at the supramolecular level (e.g., dislocation interactions, grain boundary movement, etc). However, a direct comparison between results from experiments and simulations is difficult to establish because of a significant difference in the considered strain rate. Indeed, during a typical nanoscale tensile test, the strain rate is about 10^{-2} s^{-1}, while the value usually used in simulations is several orders of magnitude higher, this being limited by the available computational resources [142]. Thus, high-strain rate experiments would be desirable in order to get further information about

the mechanical response of nanostructures, as different behavior may emerge [143] at high strain rates, which could provide a new and critical knowledge enabling high frequency electronics applications of nanomaterials, and bridge the gap between MD predictions and direct measurements.

The need for high-throughput characterization methods, which are also less fabrication- demanding, has been recently testified by the revival [103] of the buckling technique reported in [102] several years ago, for deriving the Young's modulus of ultra-thin films supported by pre-stretched compliant substrates. Indeed, the possibility to measure the wavelength of the rippled pattern induced in the specimen can be measured by optical microscopy mapping with the significant time savings.

5. Conclusions and future trends

In the last 10 years, significant advances have been reported in the field of mechanical characterization of low dimensional nanomaterials, especially with the onset of graphene and other 2D materials. On one hand, technological need continues to expand for either 1D or 2D nanomaterials because of the vast number of potential practical applications. On the other hand, technical challenges continue to persist, and those, by large, are governed by limitations in controlled production of specific nanomaterials with structural integrity and predefined properties, based on selected morphologies and geometries. Additionally, it is clear that comprehensive systematic development of metrologies and methodologies for synthesis, fabrication and testing of 1D and 2D nanomaterials is needed to advance knowledge and create databases cataloging main technological breakthroughs and advances.

To date in 1D nanomaterial arena what would presently be considered extremely valuable is ability to produce specimens with desirable properties which generally would require a control over their geometry and morphology. Number of latest studies that we reviewed in this article, portraying mechanical strength of 1D nanoscale specimens, were representative of diverse interests in 1D nanomaterials mostly because of the unparalleled theoretically predicted and experimentally attempted efforts to observe and analyze unprecedented strength of a 1D nanoscale object (nanowires or nanorods and nanotubes etc).

As it was discussed earlier for mechanical measurements of individual nanowires or nanotubes, most often they require state-of-the art high-resolution *in situ* SEM-TEM equipped with micro- or nano-manipulators, as well as custom MEMS or NEMS devices, specifically designed for a particular experiment. Similar it also true for 2D nanomaterials testing. It is not by accident that majority of reports on mechanical measurements of 2D atomically thin materials, to date, are based on an AFM enabled technique that allows for prefabricated freestanding membranes of 2D materials be readily tested without the need of picking them up from the growth/host substrate and subsequently placing them onto testing platform at an exact location and in a correct orientation.

For technology to move faster most of the fabrication, manipulation and testing steps must be streamlined, parallel and scalable, thus removing as much as possible human operation, and serial processes before and during testing. To make new technologies viable, ideally, new approaches would need to be compatible with already established semiconductor technologies and fabrication protocols, for example employing most reliable and sensitive MEMS and NEMS platforms while additionally incorporating also new emerging methods such as 3D printing, direct 3D laser writing, or any other direct writing methods. That would not only simplify, but possibly even eliminate all together the need for the nanoscale object manipulation (picking up, mounting it on testing device, aligning, imaging or exposing to high energy e-beams to ensure its position and placement), thus avoiding damage or other corruption, before testing.

Therefore the gap that needs to be filled in future, from the experimental perspective, is twofold: (a) an ability to produce (synthesize/grow) specimens with a predefined geometry/morphology and therefore with controlled desired/targeted properties, (b) establishment of standardized and well controlled methods of mechanical measurements through the development of new bottom-up reputable and reproducible fabrication approaches where specimens of interest are produced in selective, controlled predefined manner preferably using scalable high throughput methods.

ORCID iDs

Maria F Pantano https://orcid.org/0000-0001-5415-920X
Irma Kuljanishvili https://orcid.org/0000-0002-3257-2367

References

[1] Geim A K and Novoselov K S 2007 The rise of graphene *Nat. Mater.* **6** 183–91
[2] Ferrari A C *et al* 2015 Science and technology roadmap for graphene, related two-dimensional crystals, and hybrid systems *Nanoscale* **7** 4598–810
[3] Su B, Wu Y and Jiang L 2012 The art of aligning one-dimensional (1D) nanostructures *Chem. Soc. Rev.* **41** 7832

[4] Banerjee A, Bernoulli D, Zhang H, Yuen M, Liu J, Dong J, Ding F, Lu J, Dao M and Lu Y 2018 Ultralarge elastic deformation of nanoscale diamond *Science (80-.)* **360** 300–2
[5] Deng S and Berry V 2016 Wrinkled, rippled and crumpled graphene: an overview of formation mechanism, electronic properties, and applications *Mater. Today* 197–216
[6] Lee C, Wei X, Kysar J W and Hone J 2008 Measurement of the elastic properties and intrinsic strength of monolayer graphene *Science (80-.)* **321** 385–8
[7] Annett J and Cross G L W 2016 Self-assembly of graphene ribbons by spontaneous self-tearing and peeling from a substrate *Nature* **535** 271–5
[8] Walker L S, Marotto V R, Rafiee M A, Koratkar N and Corral E L 2011 Toughening in graphene ceramic composites *ACS Nano* **5** 3182–90
[9] Wang S, Cheng Y, Wang R, Sun J and Gao L 2014 Highly thermal conductive copper nanowire composites with ultralow loading: toward applications as thermal interface materials *ACS Appl. Mater. Interfaces* **6** 6481–6
[10] Novoselov K S, Geim A K, Morozov S V, Jiang D, Zhang Y, Dubonos S V, Grigorieva I V and Firsov A A 2004 Electric field effect in atomically thin carbon films *Science (80-.)* **306** 666–9
[11] Briseno A L, Mannsfeld S C B, Jenekhe S A, Bao Z and Xia Y 2008 Introducing organic nanowire transistors *Mater. Today* **11** 38–47
[12] Kaltenbrunner M *et al* 2013 An ultra-lightweight design for imperceptible plastic electronics *Nature* **499** 458–63
[13] Hu L, Kim H S, Lee J-Y, Peumans P and Cui Y 2010 Scalable coating and properties of transparent, flexible, silver nanowire electrodes *ACS Nano* **5** 2955–63
[14] Han S, Hong S, Ham J, Yeo J, Lee J, Kang B, Lee P, Kwon J, Lee S S and Yang M 2014 Fast plasmonic laser nanowelding for a Cu-nanowire percolation network for flexible transparent conductors and stretchable electronics *Adv. Mater.* **26** 5808–14
[15] Yoo E, Kim J, Hosono E, Zhou H, Kudo T and Honma I 2019 Large Reversible Li storage of graphene nanosheet families for use in rechargeable lithium ion batteries *Nano Lett.* **8** 2277–82
[16] Chen K-I, Li B-R and Chen Y-T 2011 Silicon nanowire field-effect transistor-based biosensors for biomedical diagnosis and cellular recording investigation *Nano Today* **6** 131–54
[17] Androulidakis C, Zhang K, Robertson M and Tawfick S 2018 Tailoring the mechanical properties of 2D materials and heterostructures *2D Mater.* **5** 032005
[18] Cao Y, Fatemi V, Fang S, Watanabe K, Taniguchi T, Kaxiras E and Jarillo-Herrero P 2018 Unconventional superconductivity in magic-angle graphene superlattices *Nature* **556** 43–50
[19] Ye H, Zhou J, Er D, Price C C, Yu Z, Liu Y, Lowengrub J, Lou J, Liu Z and Shenoy V B 2017 Toward a mechanistic understanding of vertical growth of van der Waals stacked 2D materials: a multiscale model and experiments *ACS Nano* **11** 12780–8
[20] Yu M, Zhao S, Feng H, Hu L, Zhang X, Zeng Y, Tong Y and Lu X 2017 Engineering thin MoS_2Nanosheets on TiN nanorods: advanced electrochemical capacitor electrode and hydrogen evolution electrocatalyst *ACS Energy Lett.* **2** 1862–8
[21] Chen Y M, Yu X Y, Li Z, Paik U and Lou X W 2016 Hierarchical MoS_2 tubular structures internally wired by carbon nanotubes as a highly stable anode material for lithium-ion batteries *Sci. Adv.* **2** 1–9
[22] Wang S, Guan B Y, Yu L and Lou X W D 2017 Rational design of three-layered TiO_2@Carbon@MoS_2Hierarchical nanotubes for enhanced lithium storage *Adv. Mater.* **29** 1702724
[23] Hacopian E F, Yang Y, Ni B, Li Y, Li X, Chen Q, Guo H, Tour J M, Gao H and Lou J 2018 Toughening graphene by integrating carbon nanotubes *ACS Nano* 7901–10
[24] Yan Z *et al* 2014 Rebar graphene *ACS Nano* **8** 5061–8
[25] Zhu Y and Chang T H 2015 A review of microelectromechanical systems for nanoscale mechanical characterization *J. Micromechanics Microengineering* **25** 093001
[26] Luo C, Wang C, Wu X, Zhang J and Chu J 2017 *In situ* transmission electron microscopy characterization and manipulation of two-dimensional layered materials beyond graphene *Small* **13** 1–18
[27] Li X, Sun M, Shan C, Chen Q and Wei X 2018 Mechanical properties of 2D materials studied by *in situ* microscopy techniques *Adv. Mater. Interfaces* **5** 1–24
[28] Akinwande D *et al* 2017 A review on mechanics and mechanical properties of 2D materials—Graphene and beyond *Extrem. Mech. Lett.* **13** 42–77
[29] Fan S, Feng X, Han Y, Fan Z and Lu Y 2019 Nanomechanics of low-dimensional materials for functional applications *Nanoscale Horizons* **4** 781–8
[30] Pantano M F, Espinosa H D and Pagnotta L 2012 Mechanical characterization of materials at small length scales *J. Mech. Sci. Technol.* **26** 545–61
[31] Read D T and Dally J W 1993 A new method for measuring the strength and ductility of thin films *J. Mater. Res.* **8** 1542–9
[32] Lu Y, Ganesan Y and Lou J 2010 A multi-step method for *in situ* mechanical characterization of 1D nanostructures using a novel micromechanical device *Exp. Mech.* **50** 47–54
[33] Liu H K, Pan C H and Liu P P 2008 Dimension effect on mechanical behavior of silicon micro-cantilever beams *Meas. J. Int. Meas. Confed.* **41** 885–95
[34] Hoffmann S, Utke I, Moser B, Michler J, Christiansen S H, Schmidt V, Senz S, Werner P, Gŏsele U and Ballif C 2006 Measurement of the bending strength of vapor-liquid-solid grown silicon nanowires *Nano Lett.* **6** 622–5
[35] Vlassak J J and Nix W D 1992 A new bulge test technique for the determination of Young's modulus and Poisson's ratio of thin films *J. Mater. Res.* **7** 3242–9
[36] Koenig S P, Boddeti N G, Dunn M L and Bunch J S 2011 Ultrastrong adhesion of graphene membranes *Nat. Nanotechnol.* **6** 543–6
[37] Zettl A and Chopra N G 1998 Measurement of the elastic modulus of a multi wall boron nitride nanotube *Solid State Commun.* **105** 297–300
[38] Wei X, Wang M S, Bando Y and Golberg D 2010 Tensile tests on individual multi-walled boron nitride nanotubes *Adv. Mater.* **22** 4895–9
[39] Song J, Wang X, Riedo E and Wang Z L 2005 Elastic property of vertically aligned nanowires *Nano Lett.* **5** 1954–8
[40] Agrawal R, Peng B, Gdoutos E E and Espinosa H D 2008 Elasticity size effects in ZnO nanowires-A combined experimental-computational approach *Nano Lett.* **8** 3668–74
[41] Brown J J, Baca A I, Bertness K A, Dikin D A, Ruoff R S and Bright V M 2011 Tensile measurement of single crystal gallium nitride nanowires on MEMS test stages *Sensors Actuators A Phys.* **166** 177–86
[42] Zhang D, Breguet J M, Clavel R, Sivakov V, Christiansen S and Michler J 2010 *In situ* electron microscopy mechanical testing of silicon nanowires using electrostatically actuated tensile stages *J. Microelectromechanical Syst.* **19** 663–74

[43] Cheng G, Chang T H, Qin Q, Huang H and Zhu Y 2014 Mechanical properties of silicon carbide nanowires: Effect of size-dependent defect density *Nano Lett.* **14** 754–8
[44] Song B *et al* 2018 Quantitative *in situ* fracture testing of tin oxide nanowires for lithium ion battery applications *Nano Energy* **53** 277–85
[45] Cheng G, Miao C, Qin Q, Li J, Xu F, Haftbaradaran H, Dickey E C, Gao H and Zhu Y 2015 Large anelasticity and associated energy dissipation in single-crystalline nanowires *Nat. Nanotechnol.* **10** 687–91
[46] Wang Q, Wang J, Li J, Zhang Z and Mao S X 2018 Consecutive crystallographic reorientations and superplasticity in body-centered cubic niobium nanowires *Sci. Adv.* **4** eaas8850
[47] Filleter T, Ryu S, Kang K, Yin J, Bernal R A, Sohn K, Li S, Huang J, Cai W and Espinosa H D 2012 Nucleation-controlled distributed plasticity in penta-twinned silver nanowires *Small* **8** 2986–93
[48] Ganesan Y, Peng C, Lu Y, Ci L, Srivastava A, Ajayan P M and Lou J 2010 Effect of Nitrogen Doping on the Nanotubes *ACS Nano* **4** 7637–43
[49] Chen L Y, He M R, Shin J, Richter G and Gianola D S 2015 Measuring surface dislocation nucleation in defect-scarce nanostructures *Nat. Mater.* **14** 707–13
[50] Cao G and Wang Y 2011 *Nanostructures and Nanomaterials* (*Synthesis, Properties, and Applications, World Scientific Series in Nanoscience and Nanotechnology*) vol 2 (Singapore: World Scientific) (https://doi.org/10.1142/7885)
[51] Morales A M and Lieber C M 1998 A laser ablation method for the synthesis of crystalline semiconductor nanowires *Science (80-.)* **279** 208–11
[52] Gomez J L and Tigli O 2013 Zinc oxide nanostructures: from growth to application *J. Mater. Sci.* **48** 612–24
[53] Wang X, Summers C J and Wang Z L 2004 Large-scale hexagonal-patterned growth of aligned ZnO nanorods for nano-optoelectronics and nanosensor arrays *Nano Lett.* **4** 423–6
[54] Mazouchi M, Poduri S and Dutta M 2014 Growth and characterization of indium oxide, zinc oxide and cadmium sulfide nanowires by vapor-liquid-solid growth technique *Appl. Phys. Res.* **6** 55–63
[55] Yang Z X, Han N, Fang M, Lin H, Cheung H Y, Yip S P, Wang E J, Hung T F, Wong C Y and Ho J C 2014 Surfactant-assisted chemical vapour deposition of high-performance small-diameter GaSb nanowires *Nat. Commun.* **5** 5249
[56] Salvetat J P, Briggs G A D, Bonard J M, Bacsa R R, Kulik A J, Stöckli T, Burnham N A and Forró L 1999 Elastic and shear moduli of single-walled carbon nanotube ropes *Phys. Rev. Lett.* **82** 944–7
[57] Yu M F, Files B S, Arepalli S and Ruoff R S 2000 Tensile loading of ropes of single wall carbon nanotubes and their mechanical properties *Phys. Rev. Lett.* **84** 5552–5
[58] Wang M S, Golberg D and Bando Y 2010 Tensile tests on individual single-walled carbon nanotubes: Linking nanotube strength with its defects *Adv. Mater.* **22** 4071–5
[59] Takakura A, Beppu K, Nishihara T, Fukui A, Kozeki T, Namazu T, Miyauchi Y and Itami K 2019 Strength of carbon nanotubes depends on their chemical structures *Nat. Commun.* **10** 3040
[60] Lu Y, Hsieh C and Su G 2019 The role of ALD-ZnO seed layers in the growth of ZnO nanorods for hydrogen sensing *Micromachines* **10** 491
[61] Anon 2009 Growth of ZnO nanowires catalyzed by size-dependent melting of Au nanoparticles *Nanotechnology* **20** 405603
[62] Greyson E C, Babayan Y and Odom T W 2004 Directed growth of ordered arrays of small-diameter ZnO nanowires *Adv. Mater.* **16** 1348–52
[63] Liu S, Liu H, Huang Z, Fang M, Liu Y G and Wu X 2016 Synthesis of β-SiC nanowires via a facile CVD method and their photoluminescence properties *RSC Adv.* **6** 24267–72
[64] Wang X, Song J, Li P, Ryou J H, Dupuis R D, Summers C J and Wang Z L 2005 Growth of uniformly aligned ZnO nanowire heterojunction arrays on GaN, AlN, and $Al_{0.5}Ga_{0.5}N$ substrates *J. Am. Chem. Soc.* **127** 7920–3
[65] Alameri D, Ocola L E and Kuljanshvili I 2017 Controlled selective CVD growth of ZnO nanowires enabled by mask-free fabrication approach using aqueous Fe catalytic inks *Adv. Mater. Interfaces* **4** 1700950
[66] Zhu G, Zhou Y, Wang S, Yang R, Ding Y, Wang X, Bando Y and Wang Z L 2012 Synthesis of vertically aligned ultra-long ZnO nanowires on heterogeneous substrates with catalyst at the root *Nanotechnology* **23** 055604
[67] Zhang L, Yan X, Jia X, Chen J, Kang L and Wu P 2017 Maximizing switching current of superconductor nanowires via improved impedance matching *Appl. Phys. Lett.* **110** 072602
[68] Song L, Myers A C, Adams J J and Zhu Y 2014 Stretchable and reversibly deformable radio frequency antennas based on silver nanowires *ACS Appl. Mater. Interfaces* **6** 4248–53
[69] Chen L Y, Richter G, Sullivan J P and Gianola D S 2012 Lattice anharmonicity in defect-free Pd nanowhiskers *Phys. Rev. Lett.* **109** 125503
[70] Richter G, Hillerich K, Gianola D S, Mönig R, Kraft O and Volkert C A 2009 Ultrahigh strength single crystalline nanowhiskers grown by physical vapor deposition *Nano Lett.* **9** 3048–52
[71] Treacy M M J, Ebbesen T W and Gibson J M 1996 Exceptionally high Young's modulus observed for individual carbon nanotubes *Nature* **381** 678–80
[72] Guo H, Chen K, Oh Y, Wang K, Dejoie C, Syed Asif S A, Warren O L, Shan Z W, Wu J and Minor A M 2011 Mechanics and dynamics of the strain-induced M1–M2 structural phase transition in individual VO2 nanowires *Nano Lett.* **11** 3207–13
[73] Zhang Y, Liu X, Ru C, Zhang Y L, Dong L and Sun Y 2011 Piezoresistivity characterization of synthetic silicon nanowires using a MEMS device *J. Microelectromechanical Syst.* **20** 959–67
[74] Zhang D, Drissen W, Breguet J M, Clavel R and Michler J 2009 A high-sensitivity and quasi-linear capacitive sensor for nanomechanical testing applications *J. Micromechanics Microengineering* **19** 075003
[75] Espinosa H D, Zhu Y and Moldovan N 2007 Design and operation of a MEMS-based material testing system for nanomechanical characterization *J. Microelectromechanical Syst.* **16** 1219–31
[76] Abbas K, Alaie S, Ghasemi Baboly M, Elahi M M M, Anjum D H, Chaieb S and Leseman Z C 2015 Nanoscale size effects on the mechanical properties of platinum thin films and cross-sectional grain morphology *J. Micromechanics Microengineering* **26** 15007
[77] Elhebeary M and Saif M T A 2017 Lessons learned from nanoscale specimens tested by MEMS-based apparatus *J. Phys. D: Appl. Phys.* **50** 243001
[78] Cao K, Han Y, Zhang H, Gao L and Yang H 2018 Size-dependent fracture behavior of silver nanowires *Nanotechnology* **29** 295703
[79] Ramachandramoorthy R, Wang Y, Aghaei A, Richter G, Cai W and Espinosa H D 2017 Reliability of single crystal silver nanowire-based systems: stress assisted instabilities *ACS Nano* **11** 4768–76
[80] Bhowmick S, Espinosa H, Jungjohann K, Pardoen T and Pierron O 2019 Advanced microelectromechanical systems-based nanomechanical testing: beyond stress and strain measurements *MRS Bull.* **44** 487–93

[81] Naraghi M, Chasiotis I, Kahn H, Wen Y and Dzenis Y 2007 Novel method for mechanical characterization of polymeric nanofibers *Rev. Sci. Instrum.* **78** 085108
[82] Anon 2016 Expanding our 2D vision *Nat. Rev. Mater.* **1** 16089
[83] Novoselov K S, Mishchenko A, Carvalho A and Castro Neto A H 2016 2D materials and van der Waals heterostructures *Science (80-.).* **353** aac9439 -2
[84] Frank I W, Tanenbaum D M, van der Zande A M and McEuen P L 2007 Mechanical properties of suspended graphene sheets *J. Vac. Sci. Technol. B Microelectron. Nanom. Struct.* **25** 2558
[85] Lin Z *et al* 2016 2D materials advances: from large scale synthesis and controlled heterostructures to improved characterization techniques, defects and applications *2D Mater.* **3** 042001
[86] Tan C *et al* 2017 Recent advances in ultrathin two-dimensional nanomaterials *Chem. Rev.* **117** 6225–331
[87] Lee G H *et al* 2013 High-strength chemical-vapor-deposited graphene and grain boundaries *Science (80-.)* **340** 1074–6
[88] Wang L, Williams C M, Boutilier M S H, Kidambi P R and Karnik R 2017 Single-layer graphene membranes withstand ultrahigh applied pressure *Nano Lett.* **17** 3081–8
[89] Zhang P *et al* 2014 Fracture toughness of graphene *Nat. Commun.* **5** 3782
[90] Pérez-Garza H H, Kievit E W, Schneider G F and Staufer U 2014 Highly strained graphene samples of varying thickness and comparison of their behaviour *Nanotechnology* **25** 465708
[91] Cao C, Daly M, Singh C V, Sun Y and Filleter T 2015 High strength measurement of monolayer graphene oxide *Carbon N. Y.* **81** 497–504
[92] Falin A *et al* 2017 Mechanical properties of atomically thin boron nitride and the role of interlayer interactions *Nat. Commun.* **8** 15815
[93] Bertolazzi S, Brivio J and Kis A 2011 Stretching and breaking of ultrathin MoS_2 *ACS Nano* **5** 9703–9
[94] Castellanos-Gomez A, Poot M, Steele G A, Van Der Zant H S J, Agraït N and Rubio-Bollinger G 2012 Elastic properties of freely suspended MoS_2 nanosheets *Adv. Mater.* **24** 772–5
[95] Liu K *et al* 2014 Elastic properties of chemical-vapor-deposited monolayer MoS_2, WS_2, and their bilayer heterostructures *Nano Lett.* **14** 5097–103
[96] Zhang R, Koutsos V and Cheung R 2016 Elastic properties of suspended multilayer WSe_2 *Appl. Phys. Lett.* **108** 042104
[97] Yang Y *et al* 2017 Brittle fracture of 2D $MoSe_2$ *Adv. Mater.* **29** 1604201
[98] Wei X, Meng Z, Ruiz L, Xia W, Lee C, Kysar J W, Hone J C, Keten S and Espinosa H D 2016 Recoverable slippage mechanism in multilayer graphene leads to repeatable energy dissipation *ACS Nano* **10** 1820–8
[99] Lee J U, Yoon D and Cheong H 2012 Estimation of young's modulus of graphene by Raman spectroscopy *Nano Lett.* **12** 4444–8
[100] Pérez Garza H H, Kievit E W, Schneider G F and Staufer U 2014 Controlled, reversible, and nondestructive generation of uniaxial extreme strains (>10%) in graphene *Nano Lett.* **14** 4107–13
[101] Davidovikj D, Alijani F, Cartamil-Bueno S J, Van Der Zant H S J, Amabili M and Steeneken P G 2017 Nonlinear dynamic characterization of two-dimensional materials *Nat. Commun.* **8** 1253
[102] Stafford C M, Harrison C, Beers K L, Karim A, Amis E J, Vanlandingham M R, Kim H C, Volksen W, Miller R D and Simonyi E E 2004 A buckling-based metrology for measuring the elastic moduli of polymeric thin films *Nat. Mater.* **3** 545–50
[103] Iguiñiz N, Frisenda R, Bratschitsch R and Castellanos-gomez A 2019 Revisiting the buckling metrology method to determine the Young's modulus of 2D materials *Adv. Mater.* **31** 1807150
[104] Nicholl R J T, Conley H J, Lavrik N V, Vlassiouk I, Puzyrev Y S, Sreenivas V P, Pantelides S T and Bolotin K I 2015 The effect of intrinsic crumpling on the mechanics of free-standing graphene *Nat. Commun.* **6** 8789
[105] Poot M and Van Der Zant H S J 2008 Nanomechanical properties of few-layer graphene membranes *Appl. Phys. Lett.* **92** 063111
[106] Zandiatashbar A, Lee G H, An S J, Lee S, Mathew N, Terrones M, Hayashi T, Picu C R, Hone J and Koratkar N 2014 Effect of defects on the intrinsic strength and stiffness of graphene *Nat. Commun.* **5** 3186
[107] Wei X, Mao L, Soler-Crespo R A, Paci J T, Huang J, Nguyen S T and Espinosa H D 2015 Plasticity and ductility in graphene oxide through a mechanochemically induced damage tolerance mechanism *Nat. Commun.* **6** 8029
[108] Suk J W, Hao Y, Liechti K M and Ruo R S 2020 Impact of grain boundaries on the elastic behavior of transferred polycrystalline graphene *Chem. Mater.* **32** 6078–84
[109] Bunch J S, Verbridge S S, Alden J S, van der Zande A M, Parpia J M, Craighead H G and McEuen P L 2008 Impermeable atomic membranes from graphene sheets *Nano Lett.* **8** 2458–62
[110] Lee J E, Ahn G, Shim J, Lee Y S and Ryu S 2012 Optical separation of mechanical strain from charge doping in graphene *Nat. Commun.* **3** 1024
[111] Lin Q Y, Jing G, Zhou Y B, Wang Y F, Meng J, Bie Y Q, Yu D P and Liao Z M 2013 Stretch-induced stiffness enhancement of graphene grown by chemical vapor deposition *ACS Nano* **7** 1171–7
[112] Cui T, Mukherjee S, Sudeep P M, Colas G, Najafi F, Tam J, Ajayan P M, Singh C V, Sun Y and Filleter T 2020 Fatigue of graphene *Nat. Mater.* **19** 405–411
[113] Christopher J W, Vutukuru M, Lloyd D, Bunch J S, Goldberg B B, Bishop D J, Swan A K and Member S 2019 Monolayer MoS_2 strained to 1.3% with a microelectromechanical system *J. Microelectromechanical Syst.* **28** 254–63
[114] Jang B, Mag-isa A E, Kim J H, Kim B, Lee H J, Oh C S, Sumigawa T and Kitamura T 2017 Uniaxial fracture test of freestanding pristine graphene using *in situ* tensile tester under scanning electron microscope *Extrem. Mech. Lett.* **14** 10–5
[115] Cao K, Feng S, Han Y, Gao L, Ly T H, Xu Z and Lu Y 2020 Elastic straining of free-standing monolayer graphene *Nat. Commun.* **11** 284
[116] Frankberg E J *et al* 2019 Highly ductile amorphous oxide at room temperature and high strain rate *Science (80-.)* **366** 864–9
[117] Nöhring W G, Möller J J, Xie Z and Bitzek E 2016 Wedge-shaped twins and pseudoelasticity in fcc metallic nanowires under bending *Extrem. Mech. Lett.* **8** 140–50
[118] Schrenker N, Schweizer P, Moninger M, Karpstein N, Mačković M, Spyropoulos G D, Göbelt M, Christiansen S, Brabec C J and Spiecker E 2019 Mechanical and electrical failure of silver nanowire electrodes: a scale bridging *in situ* electron microscopy study *Microsc. Microanal.* **25** 2038–9
[119] Liu R, Wang H and Li X 2008 A micro-tensile method for measuring mechanical properties of MEMS materials *J. Micromechanics Microengineering* **18** 065002
[120] Jiang C, Lu H, Zhang H, Shen Y and Lu Y 2017 Recent advances on *in situ* SEM mechanical and electrical characterization of low-dimensional nanomaterials *Scanning* **2017** 1985149
[121] Murphy K F, Chen L Y and Gianola D S 2013 Effect of organometallic clamp properties on the apparent diversity of tensile response of nanowires *Nanotechnology* **24** 235704
[122] Gerratt A P, Penskiy I and Bergbreiter S 2013 *In situ* characterization of PDMS in SOI-MEMS *J. Micromechanics Microengineering* **23** 045003

[123] Yilmaz M and Kysar J W 2013 Monolithic integration of nanoscale tensile specimens and MEMS structures *Nanotechnology* **24** 165502
[124] Tsuchiya T, Ura Y, Sugano K and Tabata O 2012 Electrostatic tensile testing device with nanonewton and nanometer resolution and its application to C 60 nanowire testing *J. Microelectromechanical Syst.* **21** 523–9
[125] Jayne R K, Stark T J, Reeves J B, Bishop D J and White A E 2018 Dynamic actuation of Soft 3D micromechanical structures using micro-electromechanical systems (MEMS) *Adv. Mater. Technol.* **3** 1700293
[126] Ladner I S, Cullinan A and Saha S K 2019 Tensile properties of polymer nanowires fabricated via two-photon lithography *RSC Adv.* **9** 28808–13
[127] Elhebeary M, Emon M A B, Aydin O and Saif M T A 2019 A novel technique for *in situ* uniaxial tests of self-assembled soft biomaterials *Lab Chip* **19** 1153–61
[128] Lugstein A, Greil J, Bertagnolli E, Zeiner C and Strasser G 2012 Tuning the electro-optical properties of germanium nanowires by tensile strain *Nano Lett.* **12** 6230–4
[129] Tsuchiya T, Hemmi T, Suzuki J, Hirai Y and Tabata O 2018 Tensile strength of silicon nanowires batch-fabricated into electrostatic MEMS testing device *Appl. Sci.* **8** 880
[130] Kiuchi M, Matsui S and Isono Y 2007 Mechanical characteristics of FIB deposited carbon nanowires using an electrostatic actuated nano tensile testing device *Journal of Microelectromechanical Systems* **16** 191–201
[131] Pantano M F, Speranza G, Galiotis C and Pugno N 2018 A mechanical system for tensile testing of supported films at the nanoscale *Nanotechnology* **29** 395707
[132] Han J, Pugno N M and Ryu S 2015 Nanoindentation cannot accurately predict the tensile strength of graphene or other 2D materials *Nanoscale* **7** 15672–9
[133] Cao G and Gao H 2019 Mechanical properties characterization of two-dimensional materials via nanoindentation experiments *Prog. Mater Sci.* **103** 558–95
[134] Chen L Y, Terrab S, Murphy K F, Sullivan J P, Cheng X and Gianola D S 2014 Temperature controlled tensile testing of individual nanowires *Rev. Sci. Instrum.* **85** 013901
[135] Kang W, Merrill M and Wheeler J M 2017 *In situ* thermomechanical testing methods for micro/nano-scale materials *Nanoscale* **9** 2666–88
[136] Egerton R F, Li P and Malac M 2004 Radiation damage in the TEM and SEM *Micron* **35** 399–409
[137] Pantano M F, Calusi B, Mazzolai B, Espinosa H D and Pugno N M 2019 Load sensor instability and optimization of MEMS-based tensile testing devices *Front. Mater.* **6** 161
[138] Shin J, Richter G and Gianola D S 2020 Suppressing instabilities in defect-scarce nanowires by controlling the energy release rate during incipient plasticity *Mater. Des.* **189** 108460
[139] Li C, Cheng G, Wang H and Zhu Y 2020 Microelectromechanical systems for nanomechanical testing : displacement- and force-controlled tensile testing with feedback control *Exp. Mech.* **60** 1005–15
[140] Pantano M F, Bernal R A, Pagnotta L and Espinosa H D 2015 Multiphysics design and implementation of a microsystem for displacement-controlled tensile testing of nanomaterials *Meccanica* **50** 549–60
[141] Cheng G, Yin S, Chang T H, Richter G, Gao H and Zhu Y 2017 Anomalous tensile detwinning in twinned nanowires *Phys. Rev. Lett.* **119** 1–6
[142] Ramachandramoorthy R, Milan M, Lin Z, Trolier-McKinstry S, Corigliano A and Espinosa H 2018 Design of piezoMEMS for high strain rate nanomechanical experiments *Extrem. Mech. Lett.* **20** 14–20
[143] Ramachandramoorthy R, Gao W, Bernal R and Espinosa H 2016 High strain rate tensile testing of silver nanowires: rate-dependent brittle-to-ductile transition *Nano Lett.* **16** 255–63